

# Proposal to Measure High Energy Neutrinos in Coincidence with Gamma Ray Bursts

H.J.Crawford <sup>1</sup>, Principal Investigator  
E.Anassontzis<sup>2,3</sup>, T.Athanasopoulos<sup>3</sup>, A. Belias<sup>3</sup>, F.S.Bieser <sup>1</sup>,  
J.Engelage <sup>1</sup>, C.Flagg <sup>4</sup>, A.Fotiou<sup>2,3</sup>, K.Hurley <sup>1</sup>, E.G.Judd <sup>1</sup>,  
P.Koske<sup>6</sup>, E.Markopoulos<sup>3</sup>, B.K.Lubsandorzhev<sup>8</sup>,  
K.Papageorghiou<sup>3</sup>, C.Perkins <sup>1</sup>, P.Rapidis<sup>5</sup>, L.K.Resvanis <sup>2,3</sup>, I.Siotis<sup>5</sup>,  
S.Tsagli<sup>3</sup>, A.L.Trattner <sup>1</sup>, L.F.Utkina<sup>7</sup>, G.Voulgaris<sup>2</sup>, V.A.Zhukov<sup>7,8</sup>  
<sup>1</sup>University of California, Berkeley, Space Sciences Laboratory  
<sup>2</sup> University of Athens, Athens, Greece  
<sup>3</sup> NESTOR Institute for Astroparticle Physics,  
National Observatory of Athens, Pylos, Greece  
<sup>4</sup> State University of New York, Stony Brook  
<sup>5</sup> Institute for Nuclear Physics, Demokritos, Athens, Greece  
<sup>6</sup> University of Kiel, Germany  
<sup>7</sup> Sholokov Open University, Moscow  
<sup>8</sup> Institute for Nuclear Research, Russian Academy of Sciences, Moscow

June 28, 2006

## Abstract

We propose to use a 4-floor NESTOR tower as the central element in a 4-autonomous-string + Tower *low cost omnidirectional cubic-kilometer-sized* array to detect very high-energy neutrinos in *coincidence with gamma-ray bursts*. Gamma-ray bursts are believed to have their origin in a relativistic fireball created in a hypernova and are expected to be accompanied by bursts of very-high-energy neutrinos. The neutrinos interact to produce highly radiative leptons: muons, which produce showers (catastrophic bremsstrahlung) having many km long range in water, and electrons or neutral-current events (cascades), which have short range but produce very bright showers. The two keys to our measurement are the large photon flux from the catastrophic high-energy showers and their temporal correlation with a satellite observation of the gamma-ray bursts. Our Neutrino Burst Experiment,

NuBE, also provides a complement to ICECUBE in the northern hemisphere and aids in the development of KM3NET in the Mediterranean.

The project has three phases: 1) develop the battery-powered optical modules, clocks, data acquisition, and quick-look/control acoustic system for the fully autonomous strings; 2) deploy a single battery-operated test string  $\geq 100m$  from the NESTOR tower; and 3) deploy four strings at distances of  $\geq 300m$  from the Tower to provide  $> 1km^2$  effective area coverage for the high-energy neutrinos. Current theory predicts that this size detector will observe  $\sim 10 - 100$  events per year having neutrinos of  $\sim 10^{14}eV$  in coincidence with gamma-ray bursts detected by satellites. Establishing the time correlation between  $\gamma$  and  $\nu$  may lead to new tools for astrophysical investigation of fundamental physics.

# Contents

<b>1</b>	<b>Introduction</b>	<b>8</b>
<b>2</b>	<b>Science:</b>	<b>16</b>
2.1	GRBs - Is the fireball model correct in neutrino prediction? .	16
2.1.1	Observational properties of cosmic gamma-ray bursts	17
2.1.2	The short explanation . . . . .	19
2.1.3	GRB030329 and the GRB-supernova connection . . .	20
2.1.4	The optically dark bursts . . . . .	20
2.1.5	The X-ray flashes . . . . .	21
2.1.6	GRB Conclusions . . . . .	21
2.2	Neutrino-Gamma coincidences as a tool for Particle Physics .	22
2.2.1	Obtaining Bounds on Neutrino Properties . . . . .	22
2.2.2	Relativity Principles . . . . .	23
2.2.3	Detection of Tau Neutrinos . . . . .	23
2.2.4	Neutrino Interactions . . . . .	24
<b>3</b>	<b>Status of Field of High-Energy Neutrino Astronomy</b>	<b>24</b>
3.1	Detectors in the Ice: AMANDA and ICECUBE . . . . .	24
3.2	Water Detectors - Baikal, NESTOR, Antares, NEMO, KM3NET	26
3.2.1	Baikal . . . . .	26
3.2.2	NESTOR . . . . .	27
3.2.3	Antares . . . . .	27
3.2.4	NEMO . . . . .	27
3.2.5	KM3NET . . . . .	28
3.3	SuperK . . . . .	28
3.4	GRB Satellites: SWIFT and HETE . . . . .	28
<b>4</b>	<b>Detector Requirements</b>	<b>29</b>
4.1	Description of signal . . . . .	29
4.1.1	Absolute time for satellite coincidence . . . . .	32
4.1.2	Relative time for angular correlation . . . . .	33
4.1.3	Track reconstruction for calibration on CR muons . .	33
4.2	Event rates . . . . .	34
4.3	Background rejection . . . . .	35
4.4	Calibration . . . . .	35
4.5	Monitoring . . . . .	35

<b>5</b>	<b>Optical Properties of Site</b>	<b>37</b>
5.1	Current Knowledge . . . . .	37
5.2	In situ measurement using UV LEDs + PD . . . . .	39
<b>6</b>	<b>Simulations and Detector Design</b>	<b>40</b>
6.1	Simulated Shower Signal . . . . .	40
6.2	Simulated Backgrounds . . . . .	41
6.3	Detector Design . . . . .	41
6.4	Triggering . . . . .	45
6.5	Acceptance . . . . .	46
<b>7</b>	<b>Data Analysis</b>	<b>47</b>
7.1	Data retrieval and archiving . . . . .	47
7.2	Calibration . . . . .	48
7.3	Coincidence Analysis . . . . .	49
7.4	Comparison with Satellite Data . . . . .	51
7.5	Non-GRB signals . . . . .	51
<b>8</b>	<b>Electronics</b>	<b>51</b>
8.1	Optical Modules(OM) . . . . .	52
8.2	Electronics Module (EM) . . . . .	55
	8.2.1 Digitizing Trigger Board (DTB) . . . . .	55
	8.2.2 Cluster Controller (CC) . . . . .	59
	8.2.3 Slow Controls System(SCS) . . . . .	59
	8.2.4 Data Storage System (DSS) . . . . .	59
8.3	LED Calibration Modules (LCM) . . . . .	59
8.4	Power Supplies(PS) . . . . .	60
8.5	Acoustic Modules(AM) . . . . .	61
8.6	Data acquisition(DAQ) . . . . .	61
<b>9</b>	<b>Mechanical Description of String, Node, and Cluster</b>	<b>61</b>
<b>10</b>	<b>Deployment, Operation, and Recovery</b>	<b>62</b>
10.1	Site-Measurement String . . . . .	64
10.2	Prototype String . . . . .	64
10.3	Four String + Tower array . . . . .	65
10.4	Operations . . . . .	66

<b>11 QA</b>	<b>66</b>
11.1 Single pe response . . . . .	68
11.2 DAQ tests . . . . .	68
11.3 Acoustic tests . . . . .	68
11.4 System tests . . . . .	68
<b>12 Cost and Schedule</b>	<b>68</b>
12.1 Simulations . . . . .	68
12.2 String mechanical . . . . .	69
12.3 Electronics . . . . .	69
12.4 Deployments . . . . .	69
12.5 Data analysis . . . . .	70
<b>13 Glossary</b>	<b>70</b>
<b>A Requirements</b>	<b>75</b>
<b>B Cost Sharing</b>	<b>75</b>

## List of Figures

1	NESTOR Tower . . . . .	10
2	NESTOR Floor . . . . .	10
3	Map of Methoni . . . . .	11
4	NuBE array . . . . .	13
5	CR muons vs depth . . . . .	15
6	GRB duration distribution . . . . .	18
7	Neutrino absorption in Earth . . . . .	26
8	100 TeV shower in water . . . . .	31
9	Bioluminescence at the 4km deep NESTOR site . . . . .	36
10	PMT quantum efficiency vs wavelength . . . . .	38
11	Absorption coefficient for water . . . . .	39
12	NuBE node schematic . . . . .	43
13	K40 coincidence design 1 . . . . .	44
14	K40 coincidence design 2 . . . . .	45
15	PMT coincidence rate at Nestor site . . . . .	46
16	Photon arrival-time distributions . . . . .	47
17	NuBE effective area . . . . .	48
18	Block diagram of NuBE cluster . . . . .	52
19	NuBE cluster wiring diagram . . . . .	53
20	Optical Module . . . . .	54
21	Optical transmission of housing . . . . .	54
22	Digitizing Trigger Board diagram . . . . .	57
23	Diagram of node on string . . . . .	63
24	NuBE project timeline . . . . .	69

## List of Tables

1	Burst and Afterglow Properties. The total is not 100% because of unknown contributions from neutrinos and gravitational radiations. Their contribution to the energy budget could be quite high in some cases. These numbers vary widely from burst to burst. . . . .	19
2	Some properties of high energy neutrino detectors. . . . .	25
3	Calculated light intensities of several sources contributing to the baseline rate of an optical module having a 1/4 pe threshold. . . . .	41
4	NuBE / NESTOR Detector parameters . . . . .	42
5	Data event in NuBE cluster. If we record leading and trailing edges in each PMT (3 TDC/chn, 8chn/cluster) these give 96 bytes. Since we 0 suppress, and the noise rate is low, a typical event will have only a few hits and a length of 25-30B. . . . .	49
6	Housekeeping event in NuBE cluster . . . . .	50
7	Power budget for single NuBE cluster . . . . .	60

# 1 Introduction

Gamma-ray bursts (GRB) are observed by satellites near Earth at a rate of  $\sim 1$  per day [HETE],[SWIFT]. They are believed to be among the highest energy phenomena known. The relativistic fireball model describing gamma-ray bursts has been used by Waxman and Bahcall [Waxman97] to predict a measurable flux of  $\sim 10^{14}eV$  neutrinos accompanying the  $\gamma$ -rays to Earth. According to this model, a detector of  $\sim 1km^2$  effective area will detect 10–100 neutrino-induced muon showers per year in coincidence with GRBs<sup>1</sup>. We propose to build a high-energy neutrino detector of  $> 1km^2$  effective area for  $10^{14}eV$  neutrinos within three years at a cost of  $< \$2M$  and to determine whether such neutrinos arrive in coincidence with gamma-ray bursts.

Our experiment is timely in that it coincides with satellite-borne GRB detectors expected to operate through 2010<sup>2</sup>. It also allows a technical goal in addition to our physics goal, to develop technology that may be valuable in the new KM3NET [KM3NET] detector being planned in Europe. Our autonomous strings can be used to fill in empty spaces in a large array, or to add perimeter to increase effective area, and follow the physics quickly.

GRBs were shown by BATSE data [BATSE] to have an isotropic, inhomogeneous spatial distribution. This led to a renewed credibility of models invoking a cosmological origin, but it was not until the analysis of x-ray afterglows by BeppoSax [BEPPO] that direct optical observations demonstrated this with certainty. In some cases the GRB sources were localized to hypernovae [Macfadyen]. Relativistic jets from the rapidly spinning supernova remnant interact with the relativistic shell ejecta from the original supernova event to form highly relativistic fireballs in which the gamma rays are produced by internal shocks. Local protons interact with photons to produce resonances which decay producing pions and thence very high energy neutrinos. The burst duration depends on the transit time of the jet crossing the shells.

The Neutrino Burst Experiment (NuBE) will allow us to detect  $E > 10TeV$  neutrinos from any source with an inexpensive and robust experiment, omnidirectional in sensitivity. Such sources are expected to include

---

<sup>1</sup>Other models of astrophysical processes also demand production of high-energy neutrinos, including other burst models, AGN models, and topological string models[Roy][Learned and Mannheim].

<sup>2</sup>SWIFT has just passed a 2-year NASA review and so is funded through 2008. Like all NASA missions, it is reviewed every 2 years. All expectations are that it will operate through 2010

GRBs and have a background from atmospheric cosmic ray interactions and possibly other astrophysical generators. We take advantage of the existence of both the necessary satellites [SWIFT][HETE] and the extensive NESTOR hardware, infrastructure, operating Tower, and experience to make this experiment possible. NESTOR has already investigated the site in detail [NESTOR-site] and used the Cherenkov light from high-energy muons to measure cosmic ray shower particles at the 4 km depth of the site [Aggouras1]: we expect to see a few/min/string<sup>3</sup>. Background rates ( $\sim 50kHz/PMT$  typical with 1/4 pe threshold) and bioluminescence activity (bursts to  $200kHz$ ) are well understood. These bioluminescence events are active  $\sim 1\%$  of the time as measured at the NESTOR site. NESTOR has also observed very low bio-fowling rates, low enough that these do not impact operation during our proposed one year deployments.

The NESTOR Tower shown in Figure 1 is designed to detect much lower energy neutrinos, typically 10-1000 GeV, which are expected to originate in active galactic nuclei (AGNs) [AGN], in annihilation of super-symmetric particles trapped in the sun's interior, and in local cosmic-ray interactions (Extensive Air Showers) [AUGER]. The 4-floor NESTOR Tower provides similar sensitive area to AMANDA [AMANDA], providing complementary measurements in the Northern hemisphere. The tower consists of four floors separated by 30m, with each floor having 12 photo-multiplier tubes (PMTs) on the perimeter of a 30m diameter hexagon as shown in Figure 2.

NESTOR has already successfully deployed its junction box and a single floor of the tower [Aggouras1][Aggouras2] at the site, an abyssal plane located 4km deep in the Ionian sea 15km from the Eastern coast of Greece near Methoni ( $38.6^{\circ}N, 21.7^{\circ}E$ )(see Figure 3). The single floor connects to the junction box for power and uses two of the 15 available optical fibers to send data to shore. The NESTOR Institute has a number of sea-going vessels including a triangular ship, the Delta Berenike, designed for tower and string deployments. Institute personnel are experienced in successful deployment and retrieval of hardware at the site. The optical transmission length ( $\lambda_{trans}$ ) has been measured at the site to be  $55m$  at  $460nm$  [Anassontzis94][NESTOR-site]. We will extend these in situ measurements into the UV using a series of Light Emitting Diodes (LEDs) in the region from 350-450 nm while developing the LED calibration system for NuBE. Recent measurements [Pope] suggest that  $\lambda_{trans}$  may be significantly longer than  $55m$  at lower wavelengths where the detector efficiency is highest.

NuBE adds four autonomous strings surrounding the NESTOR Tower to

---

<sup>3</sup>It takes  $\sim 2TeV$  for a muon to get down to 4km depth

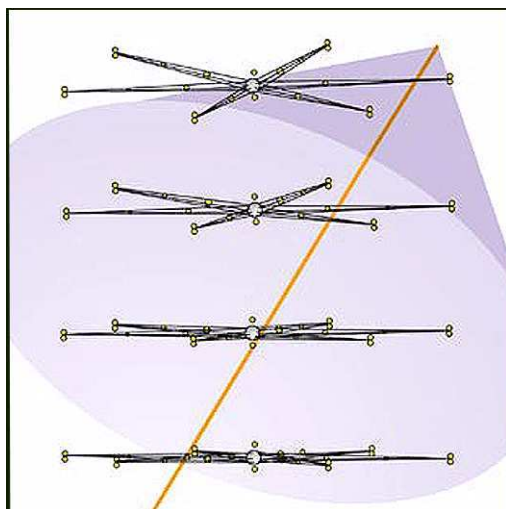


Figure 1: NESTOR Tower with 4-floors showing upward going muon and its Cherenkov cone. Each floor has 12 optical modules mounted in pairs back-to-back on the ends of the hexagonal arms.

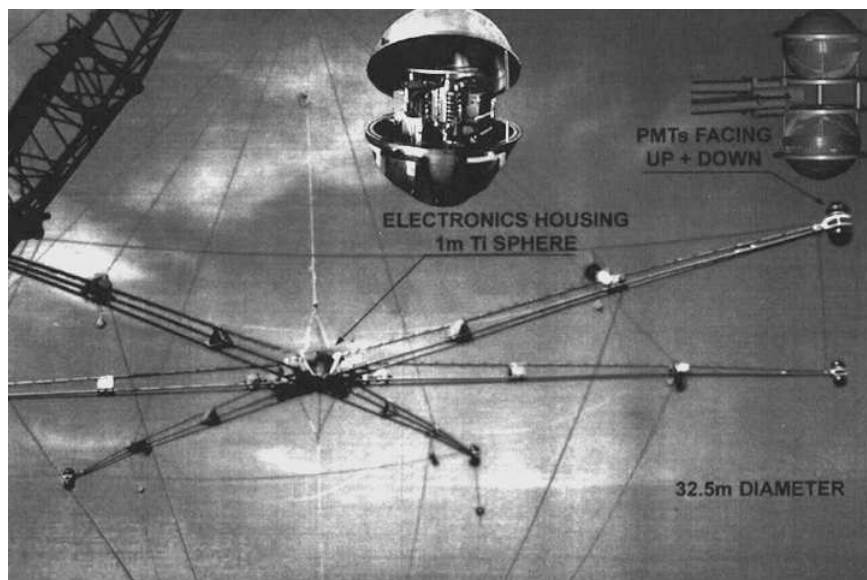


Figure 2: Picture of a single NESTOR floor – including detail of an OM and mounting of a pair of OMs.

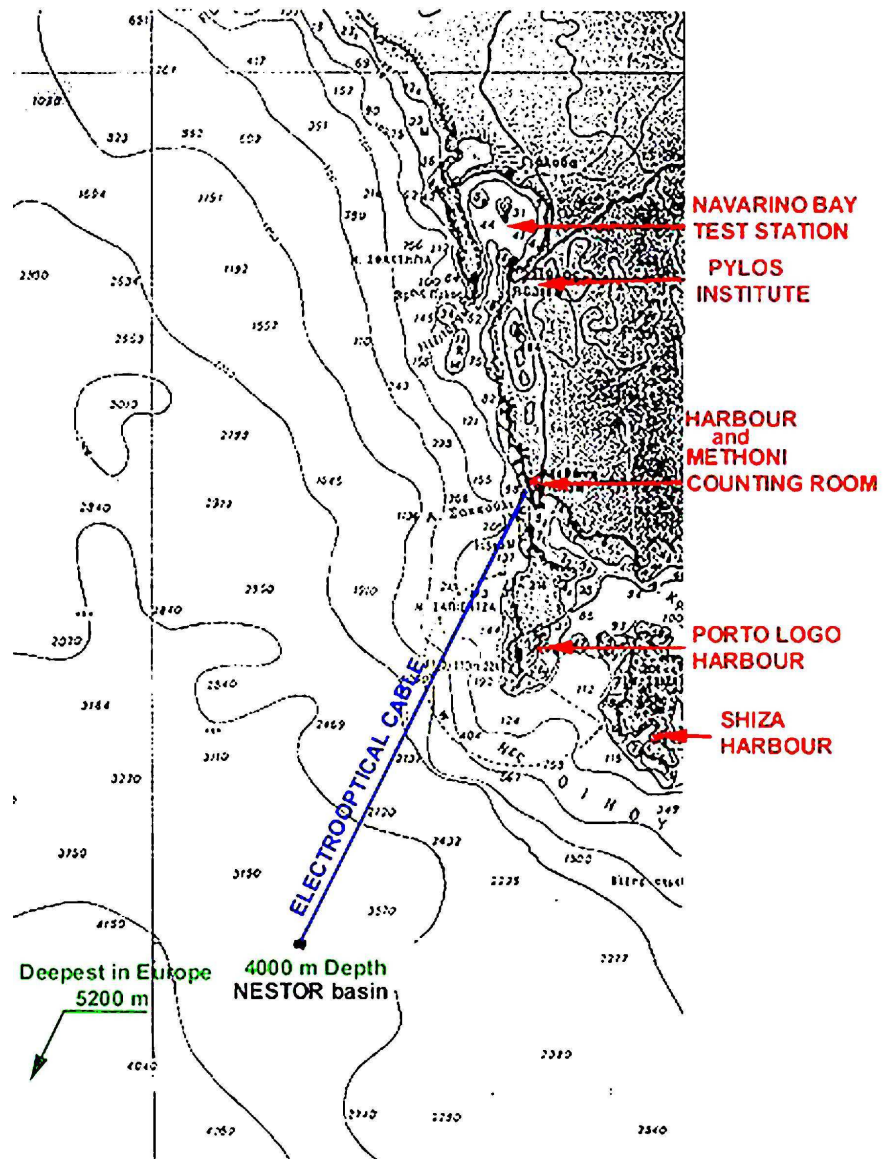


Figure 3: Map showing the site off the shore of Southwestern Greece by Methoni.

greatly increase the collecting area as shown in Figure 4. NuBE is a water-Cherenkov detector whose simple design derives from the properties of the very-high-energy leptons produced by the neutrinos. The mean energy of the neutrinos in the fireball model is  $\sim 100TeV$  [Waxman97]. Neutrino oscillations lead to equilibrium in neutrino flavor by the time they reach the Earth. Our signal consists of showering muons (catastrophic bremsstrahlung) from  $\nu_\mu$  Charged Current (CC) interactions and from muons from  $\tau$  decays produced in  $\nu_\tau$  CC interactions, or electromagnetic cascades from  $\nu_e$  CC interactions or in general Neutral Current interactions. When a high-energy muon-neutrino interacts, it typically produces a highly radiative muon, that is, a muon accompanied in its traversal of the water by many bursts of nearly collinear shower electron-positron pairs. The muon travels many km in water [Pal], producing showers of varying intensity all along its path (see Figure 8). Each minimum ionizing particle in the shower produces typically 200 Cherenkov photons per cm in the wavelength region of  $350 - 550nm$  where the quantum efficiency of the photo-multiplier tubes is good (see Section 6.3). According to our simulations of high energy showers produced along very long muon tracks in water, Cherenkov light ( $43^\circ$  angle) from this bundle of particles can be observed with high efficiency at perpendicular distances  $\geq 300m$  from the nearly collinear core tracks (see Section 6). An electron or a cascade produces a core track that is only a few meters in length, but the Cherenkov light from this short core is intense and may be seen by the proposed array at distances in excess of  $400m$ , even with a transmission length ( $\lambda_{trans}$ )  $\sim 55m$  [Anassontzis94].

The  $4\pi$  NuBE detector approximates a sphere of diameter  $\sim 1000m$ , creating an effective area of  $\geq 1km^2$  for high energy events<sup>4</sup> ( $10TeV$ ). The detector consists of four strings placed in the clear water of the Mediterranean with their anchors at the corners of a square having  $\sim 600m$  diagonals, as shown in Figure 4. The center of the array is the NESTOR Tower. Each string has two photon-detector nodes separated by  $\sim 300m$  along the string. Each NESTOR floor<sup>5</sup> and each string node acts independently having its own local clock, trigger, data acquisition and storage, thus providing robustness and redundancy. A high energy neutrino that produces a showering lepton will lead to local triggers in more than one node, with coincidence among many nodes determined by comparing local clock values off-line<sup>6</sup>. Local node clocks on different strings are periodically synchro-

---

<sup>4</sup> $4\pi(0.5km)^2 \sim 3km^2$

<sup>5</sup>we will also refer to floors as nodes in descriptions where appropriate

<sup>6</sup>The tower is considered to consist of 4 nodes in this instance

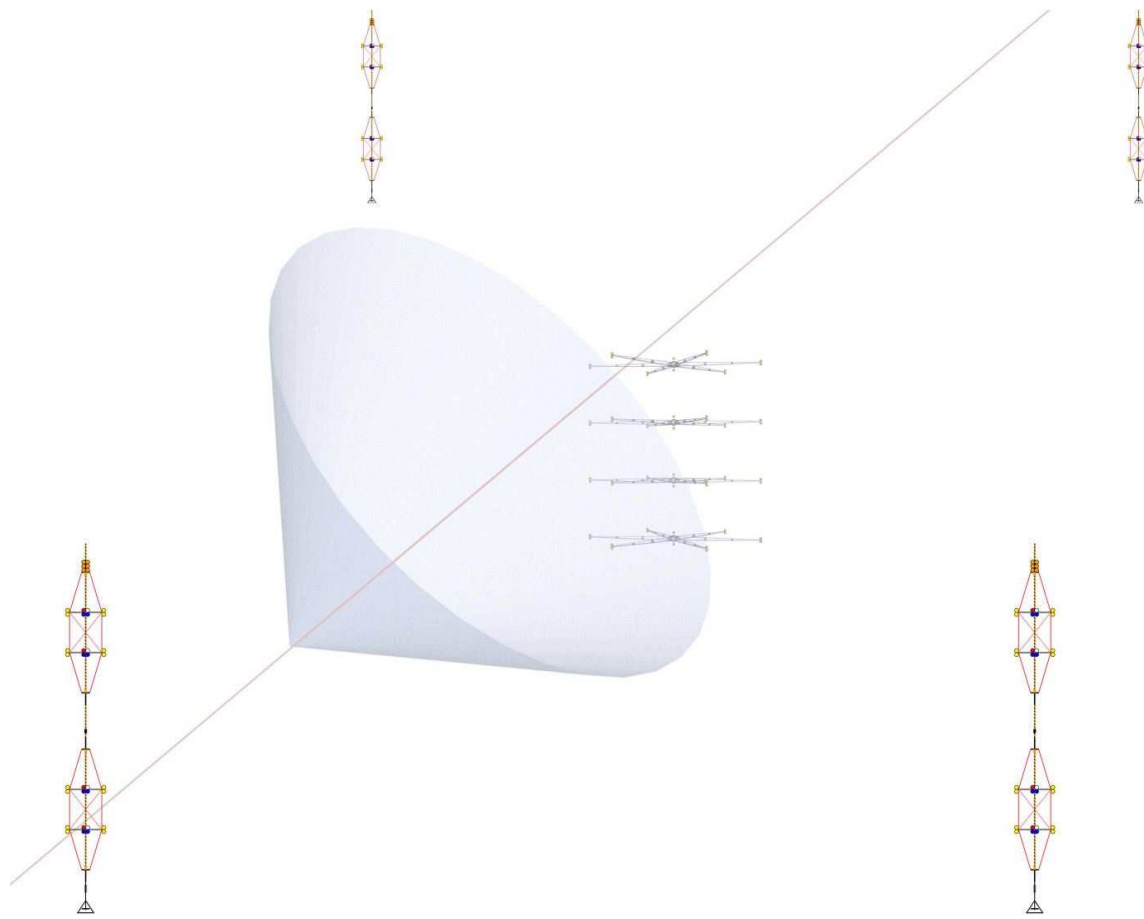


Figure 4: The NuBE array showing 4 strings surrounding the NESTOR tower. Also shown is a downward going muon with its Cherenkov cone.

nized using bright flashes of UV light from LED calibration modules near each node and on the Tower. Nodes on a single string share a common clock to minimize time drift between them. On the Tower, synchronization can also be accomplished by direct signal from shore traveling along the coax connecting floors. Absolute time is kept via the local clocks to accuracy of better than 1s per year, with relative time accurate to  $\leq 0.3\mu s$  in NuBE and  $\simeq 5ns$  in the Tower (see Section 6.3).

A signal of a high-energy event in NuBE consists of a local trigger in any node occurring within  $\sim 3\mu s$  of a local trigger in any other node. The  $3\mu s$  accounts for the muon or photon transit time across the array. The coincidence that signals the high-energy event is determined off-line. The time difference between the arrival times at each node gives the incident track direction. Events which hit three or more nodes provide redundant measures of the incident direction. Measurements made with a 12m diameter 12 PMT test floor, similar in size to one of the NuBE nodes, yielded an angle reconstruction to better than  $FWHM \sim 14^\circ$  (see Figures 6 and 9 in [Aggouras2]). This angular resolution capability provides robust verification of the correlation with the GRB: the primary identification with the GRB is based on time coincidence<sup>7</sup>. We note that measured background rates at the NESTOR site suggest that the probability of a random event falling inside the 100 s search window around the time recorded by the satellites for the GRB is  $\leq 3 \times 10^{-7}$  (see section 4.2). Our angular resolution allows us to compare to the position determined by the satellite detection as well. While most GRBs will lead to a single event in NuBE, nearby GRBs may provide more than one neutrino event in the detector, a small burst as further verification of identification with the GRB [Waxman97].

Much of the NuBE detector can be assembled from off-the-shelf items; anchors, strings, floatation, and housing spheres are items of commerce familiar to many of our collaborators. All Tower hardware and all PMTs for the four strings as well as the Tower with their pressure housings are provided by the NESTOR institute. A detailed list of components provided by NESTOR and those funded by this proposal is shown in Appendix B. Lithium-ion battery packs can provide  $> 1$  year of untended operation. The detector is easy to deploy and to recover in any of a variety of locations, since it doesn't require accurate positioning: the positions will be surveyed acoustically after deployment. The NESTOR Institute provides the Delta-Berenike and other ships as needed<sup>8</sup>. Being battery powered, the strings

---

<sup>7</sup>typical GRB duration  $\sim 10 - 100s$

<sup>8</sup>The NESTOR Institute controls a fleet of ships capable of deploying NuBE strings

have no physical connection to the Tower. Full duplex acoustic links allow communication with the Tower and thence the shore, providing a path for “quick-look” data analysis and for commands. The 4 km depth attenuates the cosmic ray muon background to  $\sim 0.1Hz$  per node, an ideal calibration rate as seen in Figure (5). Up/down discrimination within a node allows us to cross calibrate with NESTOR and with the SuperK experiment [SuperK]

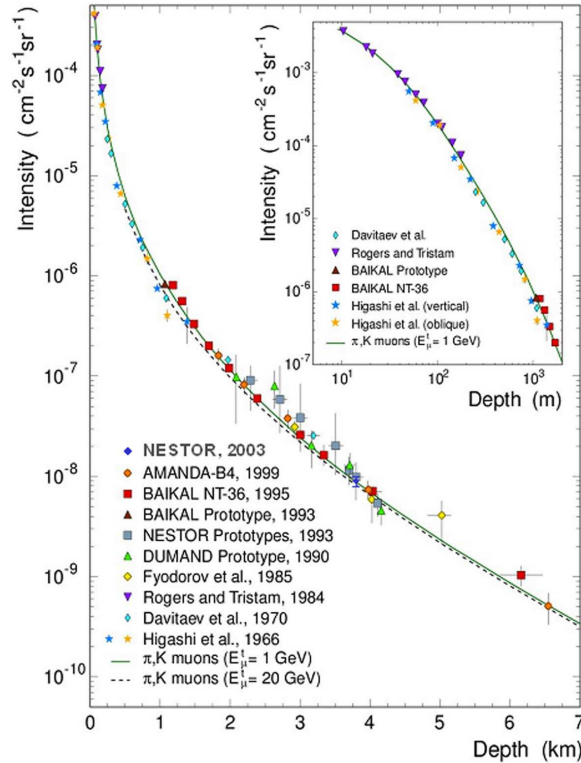


Figure 5: Cosmic ray muon background flux as a function of depth, including measurements from the NESTOR site [Aggouras1].

All deployment and recovery operations will be provided by the NESTOR Institute free of cost to this proposal. This proposal will fund our participation in the deployment activities as expert observers, tending our equipment during the operation.

Deployment plans include an in situ measurement of optical properties as a function of wavelength using recently developed LED technology during the first year of our project: the transmission length and background rates determine the geometry of the full array. The background rates and a lower

limit on the transmission length are already known at the NESTOR site [NESTOR-site], but we can measure the wavelength dependence in situ much more accurately using our UV LEDs (see Section 6.3). This will provide a detailed transmission function for use in calculating the optimal node separations and in designing the LED calibration system (see Section 8.3). Early in the second year we will deploy at least one full NuBE string, with deployment of the final 4-string array completed late in the second year of the program, as shown in the timeline of Figure 24. Using acoustic connection to the NESTOR tower we will have near-real-time access to data for the priority events (see section 6.3) and to all diagnostic monitors on the array.

Depending on local optical properties, NuBE may provide  $\gg 1km^2$  collecting area in its 4-string+tower implementation and can tell us quickly whether the fireball model is correct in its predictions of high-energy neutrino bursts. The total project, from initial approval to completion of data analysis, will take  $\sim 3$  years and cost  $\sim \$1.9M$  including contingency. We believe that the methodology developed for NuBE is easily extensible to form larger or denser arrays, and expect our autonomous string concepts to be widely used in further neutrino astronomy experiments, such as the Mediterranean Cubic Kilometer Neutrino Telescope.

## 2 Science:

The correlation of neutrinos with gamma ray bursts allows us to investigate burst models and to probe fundamental physical quantities.

### 2.1 GRBs - Is the fireball model correct in neutrino prediction?

Although there are still many mysteries surrounding cosmic gamma-ray bursts, there are nevertheless a number of well-established GRB properties with which almost everybody would agree. These are the following:

- There are at least two morphological classes of GRBs, namely the long bursts ( $\sim 20$  s duration) and the short bursts ( $\sim 0.2$  s duration).
- The redshifts and/or long-wavelength counterparts of many long bursts, and a few short bursts, have been found.
- Most of the long bursts, and some of the short bursts, display long-wavelength afterglows; but some of them have no detectable optical or radio counterparts (these are sometimes called the “dark” bursts).

- There is good evidence which links some long bursts to the deaths of massive stars.
- Some, but not all, of the short bursts originate in galaxies which have ceased to form stars long ago. This favors an origin for them in the merger of two compact objects in a binary system, but does not actually prove it.
- The energy spectra of the long bursts form a continuum: from X-ray flashes with few or no  $\gamma$ -rays, to X-ray rich bursts with some  $\gamma$ -rays, to bursts whose energy output is predominantly in the  $\gamma$ -ray range

### 2.1.1 Observational properties of cosmic gamma-ray bursts

Figure 6 shows the duration distribution of over 800 GRBs, and a fit to the distribution with the sum of two lognormal functions. The short bursts, with durations  $< 1s$ , comprise about 25% of the total, and the long bursts, with durations  $> 1s$ , about 75%. The short bursts tend to have harder energy spectra, display no spectral lag, and can be decomposed into elementary pulses which are shorter than those of the long bursts [Norris], which strongly suggests that they are generated by a different mechanism.

Until rather recently, a typical GRB energy spectrum was thought to be characterized by a peak energy  $E_{\text{peak}} \sim 200 \text{ keV}$ ; that is, all GRBs were thought to have a hard energy spectrum whose energy output was principally in the several hundred keV range. Over the years, however, evidence began to accumulate that there was another type of transient, called either an X-ray flash or an X-ray rich GRB, depending on its spectrum, whose energy output peaked in the keV or 10's of keV range, but whose other properties were identical to those of the hard-spectrum bursts ([Brand],[Stroh],[Frontera],[Sakamoto]). Today it is accepted that the energy spectra of GRBs form a continuum, from X-ray flashes, with peak energies in the 1-10 keV range, to hard-spectrum bursts, with peak energies in the several hundred keV range and above.

After the gamma-ray emission from a burst has ceased, radio, optical, and X-ray emission ensues; this is the afterglow. With sensitive detectors, the radio emission can be observed for a year or more in some cases, and the optical and X-ray emission can be observed for weeks. The optical afterglow makes it possible to identify the host galaxy of the GRB. Many have now been found, and in all cases they are normal galaxies (that is, not AGN's, for example) and are virtually indistinguishable from field galaxies at similar redshifts and ages. The nearest is at redshift 0.03, the most distant

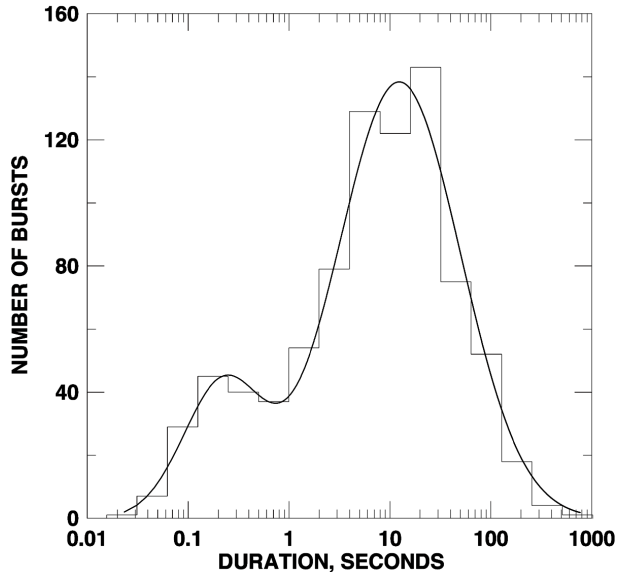


Figure 6: Burst duration distribution. Note two populations, called the short bursts, thought to originate in neutron star merging, and the long bursts, thought to originate in hypernovae.

at redshift 6.3, and the average of the distribution is 1.9. It should be kept in mind that this is a *measured* distribution, uncorrected for any selection effects. A few X-ray flash redshifts have been measured (e.g. [Soderberg]) and they are well below the average.

Knowing the distances allows an estimate of the isotropic gamma-ray energy; it ranges from  $> 10^{51}$  to  $> 10^{54}$  erg. While many sources of energy have been proposed over the years, only two are still discussed in detail. One is merging compact objects, such as two neutron stars in a binary system; this has been proposed as a source of short-duration bursts ([Perna]). The other is collapsars (also called hypernovae, or energetic supernovae - [Macfadyen]); this is proposed as a source of the long bursts. In both models however, the total energy liberated is well below  $10^{54}$  erg in  $\gamma$ -rays, so the models invoke beaming.

There is observational evidence in afterglow light curves that it indeed occurs in some cases. The evidence comes from a “break” which is often observed in the decay of the optical afterglow. This is interpreted as the point at which a narrowly collimated, hyper-relativistic jet begins to slow down, and expands into a larger solid angle. By timing the occurrence

Spectrum	Bursts	Afterglow
> 25 keV $\gamma$ -rays	65% of EM energy	7%
1 – 10 keV X-rays	7%	9%
optical	0.1%	2%
radio	unknown	0.05%
Mev/Gev/Tev neutrinos	?	
Gravitational radiation	?	

Table 1: Burst and Afterglow Properties. The total is not 100% because of unknown contributions from neutrinos and gravitational radiations. Their contribution to the energy budget could be quite high in some cases. These numbers vary widely from burst to burst.

of the break, the jet opening angle can be obtained in a model-dependent way ([Frail01]). In addition to reducing the energy requirement, beaming can turn GRBs into standard candles, again in a model-dependent fashion [Frail01]. In this interpretation, the jet opening angles range from  $1^\circ$  to  $25^\circ$ , and the average is  $4^\circ$ . In a more refined analysis [Bloom] the average energy in a GRB is found to be  $1.3 \times 10^{51}$  erg.

The total energy in a burst and in the afterglow is distributed over the electromagnetic spectrum roughly as shown in Table 1. These numbers have been derived from various bursts, and there is considerable variation from burst to burst. There have been no measurements of the non-electromagnetic emissions from bursts, but there is considerable speculation that neutrinos of all energies and gravitational radiation could account for a very large amount of energy, orders of magnitude greater than the electromagnetic energy [Vanputten].

### 2.1.2 The short explanation

The following picture is based on observations of the long GRB's, their afterglows, and their host galaxies. A GRB occurs in the star-forming region of a galaxy at a redshift of about 1 – 2. In currently popular models, it is caused by the collapse of a massive star ( $\approx 30$  solar masses) which has exhausted its nuclear fuel supply. The star collapses to a black hole threaded by a strong magnetic field, and energy is extracted through the Blandford-Znajek mechanism [Blandford]. This energy goes into accelerating shells of matter, once part of the massive star, to ultra-relativistic velocities (Lorentz factors of several hundred). These shells collide with one another as they

move outward, producing “internal” shocks. The shocks accelerate electrons and protons, and the electrons emit synchrotron radiation. In the observer’s frame, the synchrotron radiation appears in gamma-rays. The protons absorb photons to form  $\Delta$  resonances, which decay to give ultra-relativistic  $\nu$ s.

The explanation for the short bursts is not as clear. Some of them appear to occur at the outskirts of nearby galaxies which have ceased star formation. This favors an explanation which invokes old objects, such as two neutron stars, or a neutron star and a black hole, in a binary system. However, the “short” bursts sometimes display extended soft emission, lasting for about 100 s, which is difficult to explain in the merger model. And some short bursts are found in star-forming galaxies. Although this does not rule out the merger model, it does add to the number of possible explanations. Gravitational wave emission (which is now in principle within the sensitivity limit of LIGO) and neutrino emission are often cited as the keys to unlocking this important remaining GRB mystery.

### 2.1.3 GRB030329 and the GRB-supernova connection

GRB030329 was a very bright burst, in the top 1% of all bursts observed to date [Vanderspek]. It was also nearby ( $z=0.17$ , [Matheson]), and is the best-studied GRB to date, with well over 100 observations at various wavelengths. Both its optical afterglow light curve and spectrum display strong evidence for an underlying supernova component. The light curve can be decomposed into two components: a monotonic power law decay, which is characteristic of GRB afterglows in general, and a supernova-like light curve, which dominates the emission starting around 20 days after the GRB. The supernova has been named SN2003dh. The optical spectrum of SN2003dh is comparable to that of SN1998bw. SN1998bw was a peculiar type Ic supernova, which may have been associated with GRB980425 ([Galama98a]). Although these supernova signatures have now been observed in numerous GRBs, GRB030329 is the most convincing case to date.

### 2.1.4 The optically dark bursts

35% of the GRBs detected by BeppoSAX had no detectable optical counterparts ([Piro]), and several suggestions have been put forward to explain this. One is that the optical light is absorbed by dust within the host galaxy. Another is that, for some reason, the light curve is intrinsically faint and/or rapidly fading. A third is that some bursts may be at very high redshifts.

Today, the first two suggestions have been confirmed by observations. Although the third idea has not been confirmed, there could obviously be selection effects, since if an optical counterpart is not observed, it is very unlikely that a burst's redshift will be measured.

Only  $\sim 10\%$  of the bursts detected by the HETE spacecraft are optically dark. One of the big differences between the BeppoSAX and HETE missions is that, by design, HETE gets GRB positions out to astronomers faster than BeppoSAX was able to. Thus more faint or rapidly fading afterglows are likely to be detected in response to HETE burst alerts. And the Swift mission has made it possible to produce arcsecond positions within minutes of a burst, reducing still further the percentage, although not to zero.

### 2.1.5 The X-ray flashes

Several explanations have been advanced to explain the X-ray flashes, which are like GRBs in every respect except for the gamma-rays. One is that they are GRBs observed away from the jet axis, where the Lorentz factors are much lower. A second is that they are explosions with less relativistic ejecta. A third is that they are GRBs at very high redshifts. Determining whether or not these have correlated neutrinos would greatly aid our understanding of these bursts.

In the case of XRF020903 ( $z=0.251$ ), Soderberg et al. [Soderberg] have argued that the explanation lies in the amount of relativistic ejecta. This in turn suggests that XRFs are closely related to GRBs. Another piece of evidence which supports this idea is the  $E_{\text{peak}}-E_{\text{isotropic energy}}$  relation. This was first noted by Amati et al. [Amati], who found by studying the BeppoSAX bursts with known redshifts that the peak energy in a GRB spectrum is related to its isotropic equivalent energy:  $E_{\text{peak}} \propto E_{\text{iso}}^{0.52}$ .

Lamb et al. [Lamb] have begun to extend this relation down to the XRFs using HETE results. They find that the relation holds also for XRFs, which are an extension of the Amati relation down to small values of  $E_{\text{peak}}$ . While there are several possible explanations for just why this relation should hold, the fact that XRF's and GRB's lie along the same curve strongly suggests that XRFs and GRBs are similar phenomena.

### 2.1.6 GRB Conclusions

The main conclusions to draw from the current state of our knowledge of cosmic gamma-ray bursts are the following:

- Good evidence now links some of the long GRBs to Type Ic supernovae and therefore to the deaths of massive stars.
- Good evidence suggests that the short bursts indeed form a separate class, and that some may be generated in compact object mergers which are relatively nearby compared to the long bursts.
- The mystery of the dark bursts is being solved, but the question remains open whether some of them are at high redshifts.
- GRBs are bright enough to be detected out to  $z > 10$ , and even beyond. Such bursts could have been generated by the first generation of massive stars. Detecting them is one of the goals of the Swift mission.
- The search for non-electromagnetic emission associated with GRBs has been underway with experiments such as AMANDA and LIGO. **The detection of such emission would provide a unique key to the understanding of the initial moments of the burst.**

Detection of UHE neutrinos in coincidence with GRBs would corroborate the cosmological fireball scenario, and offer an important piece of evidence for solving the short GRB mystery.

## 2.2 Neutrino-Gamma coincidences as a tool for Particle Physics

It is important to maximize the physical inferences that can be drawn from coincident photon and neutrino detection [Weiler]. Fundamental topics include determination of neutrino mass<sup>9</sup> and test of the equivalence principle for neutrinos.

### 2.2.1 Obtaining Bounds on Neutrino Properties

The large distances, short emission time, and trajectory through varying gravitational fields, leads to the potential for tests of some fundamental neutrino properties not possible in terrestrial laboratories [Weiler]. Limits can be placed on neutrino mass, lifetime, electric charge, and neutrino oscillation parameters.

---

<sup>9</sup>from those events for which the source distance is known

### 2.2.2 Relativity Principles

The simultaneous observation of neutrinos and gamma rays from cosmological sources would provide us with a unique probe of space-time on intergalactic scales. The proposed array can measure absolute time to significantly better than 1s accuracy over a period of one year. The photon flight time from a source at 100 Mpc distance is  $10^{16}$  seconds: the 1s accuracy on the absolute arrival time of gamma-rays and neutrinos provides an accuracy of  $\sim 10^{-16}$  in our determination of relative velocity between neutrinos and gamma-rays. For longer bursts, the burst duration sets the limiting accuracy to perhaps  $\sim 10^{-15}$ . This measurement yields a very high precision test for special relativity and for the weak equivalence principle (WEP), a fundamental postulate of general relativity and other metric theories of gravity.

According to the WEP, the photons and neutrinos should suffer the same time delay as they pass through a gravitational potential. If the most influential gravitational potential along the path is the local galaxy, we can compute a time difference that would result from various trajectories with respect to the galactic nucleus, the suspected site of a black hole. NuBE detection of GRB neutrinos would allow a test of the weak equivalence principle to an accuracy of  $10^{-7}$  [Weiler]. Results from measurements on low energy neutrinos from the supernova 1987a probed this value to  $10^{-2}$  ([Krauss], [Longo87]). On the other hand, the most influential gravitational potential sampled may be near the source itself. If we see nearly the same delay for all GRB events regardless of distance this may point to a failure of general relativity in predicting the exit time from the source [Weiler].

### 2.2.3 Detection of Tau Neutrinos

Detection of Tau neutrinos would imply neutrino oscillations in transit. The key signature is the charged current  $\nu_\tau$  interaction, which produces a double cascade, one from hadrons produced in the interaction  $\nu_\tau q \rightarrow \tau + x$  and one as the produced  $\tau$  lepton decays to hadrons. At  $10^{14}eV$  the  $\tau$  travels only a few cm before decaying<sup>10</sup>. Tau neutrinos could theoretically be identified by the double bang events [Pakvasa] at much higher energy but the two individual bangs would be very difficult to resolve in the proposed detector.

---

<sup>10</sup>For the  $\tau$ , the  $c\tau = 87microns$ , mass=1.888 GeV,  $\gamma(100TeV) \sim 5 \times 10^4$ .

### 2.2.4 Neutrino Interactions

Improving knowledge of the partonic structure of the nucleon has made possible a series of increasingly refined predictions for the neutrino interaction cross sections. The cross section calculations are based on the CTEQ parton distributions within a nucleon [Ghandi98] .

Given a neutrino flux at Earth we can calculate a muon signal using an Earth model and the neutrino interaction cross sections. We must extrapolate using our interaction model up to  $100\text{TeV}$  and beyond. If we find neutrino correlations in NuBE, we can imagine expanding the detector to allow detailed studies of these high-energy cross sections.

## 3 Status of Field of High-Energy Neutrino Astronomy

There are a number of active efforts to construct high energy neutrino telescopes for astrophysical observation including AMANDA (begun in 1992) and ICECUBE at the South Pole, BAIKAL (begun in 1987) at Lake Baikal in Russia, and ANTARES (begun in 1997), NEMO in Italy, and KM3NET in the Mediterranean with the site to be chosen in 2009-2010. The NESTOR experiment began in 1994. Characteristics of these arrays are shown in Table 2. All of these experiments require knowledge of the neutrino-nucleon interaction cross section to interpret their signals. Our investigation also requires satellites such as Swift [SWIFT] and HETE [HETE] to be operating to detect GRBs during our period of deployment. The SWIFT satellite is expected to operate until 2010; no GRB satellites are on the books to replace SWIFT, making the next four years a window of opportunity for our GRB-neutrino coincidence measurements.

As noted above, the NESTOR array forms an integral part of NuBE, and NuBE can be viewed as a simple extension of NESTOR with greatly simplified scientific goals. NESTOR has published numerous papers on the signal detected at 4km depth at the site, giving NuBE an excellent foundation.

### 3.1 Detectors in the Ice: AMANDA and ICECUBE

AMANDA [AMANDA] and ICECUBE [ICECUBE] , located  $\sim 1.4 - 2.4\text{km}$  deep in the ice near the South Pole, are densely instrumented arrays designed for single-track pointing to identify point sources. Amanda-II has investigated GRB signals, finding none in their 3-year search, and setting an upper limit on the Waxman-Bahcall type flux well above the prediction

Detector	Status	Depth
AMANDA(ice)	operating	1450-2000m
ANTARES	1 string operating	2200 m
BAIKAL NT-200	operating	1070 m
ICECUBE(ice)	9 strings op	1450-2450m
KM3NET	R&D	
NEMO	R&D	
NESTOR	1 floor op.	4km
SUPER K	operating	
NuBE	proposed	4km

Table 2: Some properties of high energy neutrino detectors.

[AMANDA]. The relatively dense instrumentation of these ice detectors is intended to determine source origin by pointing back to the neutrino trajectory with a  $\sim 1^\circ$  accuracy [ICECUBE]. Dense instrumentation is needed to offset the effects of scattering in the ice. When ICECUBE is complete in 2010+<sup>11</sup> it is expected to have a total effective area of  $\sim 1.2km^2$  for upward going neutrinos at  $10^{14}eV$ . Its sensitivity to downward going neutrinos depends on the scattering in the ice since its PMTs all point downward, and the effective area described in their paper for the interval 100TeV-1 PeV is dominated by the higher energy signals. Our area is larger in part because of the scattering in the ice: many of the photons generated in the shower are scattered making them inefficient in their trigger. Our electronics is based on a much simpler time-to-digital converter: ICECUBE Uses a waveform digitizer that preserves much more information than our simple edge counters. Our TDC sensitivity of 2.5ns is smaller than their quoted resolution of 7ns [ICECUBE]: they have obtained in practice  $\leq 5ns$  [ICECUBE1].

Having their photomultiplier tubes pointing only downward, these detectors are nearly blind to the highest energy neutrinos because of absorption in the Earth, as shown in Figure 7, although the loss at  $10^{14}eV$  is small. Being located on the South Pole they see only a portion of the sky. NuBE proposes to make a larger array that is omnidirectional having a  $4\pi$  effective area  $\gg 1km^2$ .

NuBE is a sparse detector to look specifically for neutrinos of  $\sim 100TeV$  and to determine whether they are in time coincidences with the GRBs.

---

<sup>11</sup>it is not clear that there will be satellite coverage for GRBs by the time it is completed

NuBE is a much simpler detector to build since we do not intend to obtain high directional accuracy and we are only interested in very high energies where the muons are catastrophically radiative. Concentrating on radiative muons and electrons and relaxing the pointing requirements mean that we are relatively insensitive to scattering effects as long as the optical scattering cross section is not large enough to destroy the  $\mu s$  time coherence. The scattering length in the deep ocean water has been measured to be many hundreds of meters. In addition, the NuBE detectors can be easily deployed and recovered, unlike the detectors operating in the ice.

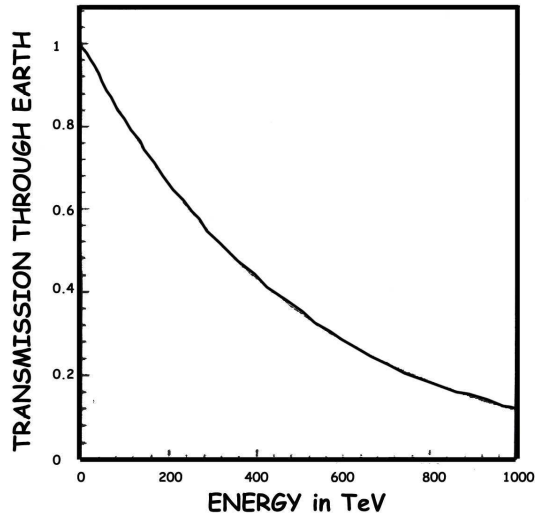


Figure 7: Transmission probability for high energy neutrinos passing diametrically through the Earth. [Ghandi98]

## 3.2 Water Detectors - Baikal, NESTOR, Antares, NEMO, KM3NET

### 3.2.1 Baikal

The detector in Lake Baikal, Russia, is launched and repaired each winter for the period that Lake Baikal is frozen, typically 8 weeks per year. They have the advantage of water, being able to retrieve their instrument for repair, but only when the ice is well frozen, since this forms their operating platform. Baikal has reported results on cosmic ray muon flux [BAIKAL]

at their depth ( $\sim 1km$ ), and a few neutrino signals. They are recently experimenting with adding 3 auxiliary strings at distances of 60m from their central NT-200 array, specifically to increase the collection area, and we list their NT200+ parameters in Table 2. Baikal also uses photomultiplier tubes in glass spheres on strings, powered from shore. Their PMTs also point only downward because of very high sedimentation rates. Note that their depth constrains the amount of target material above them; their effective volume for  $10^{14}eV$  is not spherical. Since their PMTs point downward, they see the target material above them only by scattering.

### 3.2.2 NESTOR

NESTOR is a Mediterranean detector operating at a depth of 4000m. It is designed as a tower of 12 floors of PMTs, 12 PMTs (15" diameter) per floor as shown in Figure 2 with its PMTs looking both up and down. NESTOR has deployed and taken data with one floor. They have published their results in NIM [Aggouras1] and in Astroparticle Physics [Aggouras2]. Four floors will be ready for deployment in May 2007. Nestor has already measured the cosmic ray flux and zenith angle distribution at 4km depth, so we know what our basic signal and noise will be for each node. The Nestor site is the primary candidate for KM3NET: therefore our innovations will be well scrutinized and will likely find a place in the large, dense instrument being designed.

### 3.2.3 Antares

The ANTARES collaboration has adopted the string concept which was initiated by DUMAND [DUMAND]. They operate in the Mediterranean at a depth of 2500m near Toulon, France. Due to the high sedimentation rate they only have the PMTs looking downward. In March 2006 they connected to the umbilical and operated one string successfully with 75 PMTs (10" diameter) [ANTARES].

### 3.2.4 NEMO

This is an R&D project to be located at a depth of 3500m 100km southwest of Capo Passero in Sicily [NEMO]. They plan to deploy in 2006 a minitower with a total of 16 PMTs attached at the ends of four 15m long aluminum struts.

### 3.2.5 KM3NET

The European Union recently (February 2006) funded with 9M Euros a three year Design Study (total budget 20M Euros) in which 36 institutions participate from eight European Union countries. The charge is to study the designs for a cubic kilometer size neutrino telescope to be located in the Mediterranean, with the site to be chosen after the end of the design study. The major objective is to come up by 2009 with the Technical Design Report of the cubic km telescope with a ceiling on the overall cost of 200M Euros (excluding personnel). The backbone of the KM3NET consortium is formed by participants of the NESTOR, ANTARES and NEMO experiments. It should be noted here that the recent recommendation to the European Commission of the ESFRI<sup>12</sup> Expert Group on Astronomy, Astrophysics, and Astroparticles is that KM3NET be part of the roadmap of large facilities to be funded by Framework Program7 along with the Extremely Large Telescope and the Square Kilometer Radio Array. All three infrastructures were recommended with the same priority.

### 3.3 SuperK

The SuperK neutrino detector is very densely instrumented to study low energy neutrinos and proton decay. SuperK is very efficient at detecting GeV neutrinos, those giving rise to muons having ranges of a few of meters, the contained events. This “known flux” through its  $1000m^2$  effective area provides an excellent guide to what we should be able to see in individual nodes of NuBE. The upper limit for measurable energy is  $\sim 20GeV$ .

### 3.4 GRB Satellites: SWIFT and HETE

Our experiment requires measurement of the GRB times on satellites such as Swift [SWIFT] and HETE [HETE]. These instruments are expected to take data through 2010. BATSE [BATSE], which began the GRB field, and BEPOSAX [BEPP0], which facilitated investigation of the afterglow properties which strongly support the hypernova model, are no longer operating. The GLAST mission is expected to launch by 2008, but it does not have the capabilities of SWIFT - its mission is complementary to SWIFT. The GLAST burst monitor is much smaller, and the satellite can slew only slowly to the direction of detected bursts, meaning that it will miss bursts and miss the afterglow analysis important for positive identification. The

---

<sup>12</sup>European Strategy Forum on large Research Infrastructures

robust detection of GRBs and analysis of time correlation with neutrino detection requires an instrument such as SWIFT to be efficient.

## 4 Detector Requirements

Our measurement technique is to use large-photocathode-area photomultipliers<sup>13</sup> to detect arrival time of Cherenkov photons generated in 4km deep water by “extensive water showers” initiated by high-energy neutrino interactions. Our approach differs in that our detectors are battery-powered for simple deployment and they use extremely low power electronics and data storage. Since our goal is detection of the high-energy neutrinos in coincidence with the satellite GRB detection, our detector can be simply a reliable trigger for an accurate clock. Our measurement of “hit” times at each PMT are much better than needed and are sufficiently accurate to allow reconstruction of single tracks for calibration on lower energy muons.

### 4.1 Description of signal

When a high-energy neutrino interacts with a quark in a nucleus or scatters off an electron it can produce a relativistic charged lepton. The flavor of the lepton depends on the flavor of the incident neutrino. If the neutrinos originate in charged pion decay we expect twice as many muon neutrinos as electron neutrinos and no tau neutrinos. However, lepton flavor oscillation will change this mix to flavor equality in transit. While the neutrinos act only through the weak force and are effectively invisible, the charged leptons they produce interact electromagnetically as well and are visible through their Cherenkov (Ck) radiation, and so do the showering particles of the neutral current interaction.

Cherenkov light is produced when a charged particle traverses a medium at a speed greater than the local speed of light,  $c/n$ , where  $c$  is the speed of light in vacuum, and  $n$  is the index of refraction. The number of photons generated at a wavelength  $\lambda$  in traveling a distance  $x$  at a speed  $\beta c$  is

$$\frac{d^2N}{d\lambda dx} = \frac{2\pi\alpha}{\lambda^2} \left[ 1 - \frac{1}{\beta^2 n^2(\lambda)} \right] \quad (1)$$

These photons are generated on the surface of a cone which spreads out from the particle trajectory with an opening angle given by

$$\theta_c = \arccos(1/n\beta) \quad (2)$$

---

<sup>13</sup>Hamamatsu R2018 15” diameter, 2200cm<sup>2</sup> photocathode area

as depicted in Figure 4. For our particles,  $\beta \sim 1$  and, for water,  $n \sim 1.33$  so  $\theta_c \sim 43^\circ$ . As seen from equation 1 the spectrum is weighted toward the ultra-violet where there is still considerable disagreement about the effective absorption length of water [Litjens]. Our signal consists of  $\sim 200$  photons in the range of 350-550 nm spreading out in a cone from each cm of trajectory of each relativistic particle.

NuBE is designed to observe cascade or shower events, not single muon tracks. When we confine our search to very-high-energy neutrinos, we are dealing with leptons that are highly radiative. These produce many e+e- pairs through accompanying catastrophic Bremsstrahlung photons, developing showers of particles in the water ( $L_{radiation-length} \sim 36cm$ ), as shown in Figure 8. Each of these produced shower electrons or positrons is itself a Cherenkov emitter, as well as a potential shower seed, so that the amount of Cherenkov light emitted by each neutrino-produced lepton is much larger than the light emitted by a single relativistic particle.

The high-energy muons produced by  $100TeV$  neutrino interactions have ranges in water of many km, as calculated using equation 3.

$$Range = 4.0 \ln(1 + E/1TeV) km \quad (3)$$

At 10 TeV, the mean range for a muon shower in water is  $\sim 9km$  [Pal]; at 100 TeV it is  $\sim 18km$ . To estimate the number of particles in the shower we can divide the total energy by the range and by the mean energy loss rate for a minimum ionizing particle: for 100 TeV,  $N \sim 10^{14}eV / (18 \times 10^5 cm \times 10^6 eV/cm) = 60$  particles on average in the shower bundle. Our GEANT simulations of 100 TeV muons indicate an equivalent average of 77 shower particles<sup>14</sup> accompany the muon along its whole path: the light output is nearly equivalent to 77 collinear particles rather than the single muon. A  $10^{14}$  eV muon may produce long-duration signals in our detector, much longer than the virtually instantaneous signal from a single track as light from off-axis particles produced earlier in the shower propagates to the detectors at the relatively slow speed-of-light in the water.

If a  $10^{14}eV$  electron neutrino is incident or a neutral current interaction occurs, the electrons produced by such neutrinos have short range but very intense showers acting like a flashlight. An EGSnrc [EGS] simulation indicates a 100 TeV electron produces a shower of  $< 10m$  in length having a broad maximum with  $> 40k$  particles in the shower. Tau leptons would have a “double bang” signature: NuBE may detect these, but will not be able to resolve the two pulses at  $100TeV$  energy because the two bangs

---

<sup>14</sup>typically electrons having energy  $\geq 1.5MeV$

are too close together. The neutral current interaction produces copious  $\pi^0$  which form cascades just like those initiated by electrons, and these are likely indistinguishable in NUBE: the fact that only half the  $\nu$  energy forms hadronic debris is not a problem since it still leads to a visible signal in our detector. We take advantage of the long distance coherence of the signals - we expect a single shower to trigger multiple nodes separated by 300m or more - to justify construction of a very sparsely populated, hence simple and inexpensive, detector array.

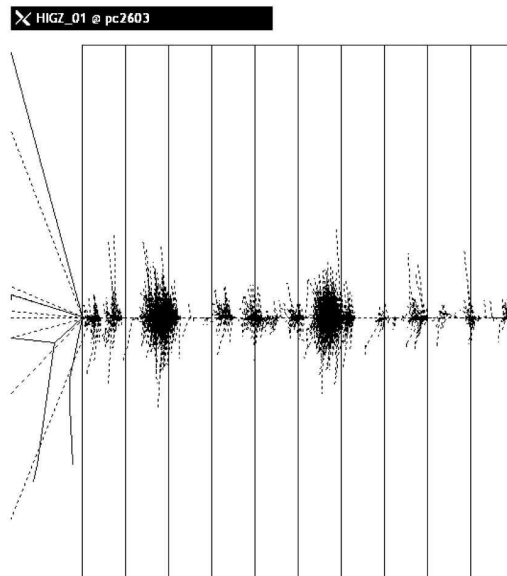


Figure 8: 100TeV muon in water. 10 meter grid showing catastrophic Bremsstrahlung showers. The vertical scale is 1 m total, showing that the accompanying particles are virtually collinear with the core track.

NuBE will also be sensitive to individual relativistic particles, but with a much smaller effective area because of the lower light level from a single track. Downward going cosmic ray muons will dominate our single string signals (see section 6.3), although we are protected by the great depth of the detector as shown in Figure 5. Upward going single muons and electrons originating in lower energy neutrino interactions below the detector will also be detectable with a similar effective area. Our timing will be accurate enough to distinguish upward from downward going particles. If there were no absorption or scattering in the water, a single one of the proposed detector nodes would record typically  $\geq 3$  photo-electron (p.e.) hits from a single

relativistic track at a distance of more than 300m.<sup>15</sup> It is important to note that NuBE will detect high-energy neutrinos if they exist, regardless of whether they are in coincidence with the GRBs, but NuBE is not intended to measure lepton energy spectra.

Once we have detected signals from neutrinos (multi-node, time ordered signals), it remains to determine whether these events are correlated with GRBs. Requiring that events be in coincidence with gamma-ray bursts constrains both arrival time and direction of the neutrinos.

#### 4.1.1 Absolute time for satellite coincidence

The longest duration GRB observed has duration  $\sim 100s$ , with a typical duration of  $\sim 20s$  (see Figure 6). This puts a constraint on when in absolute time the neutrino detector must see a signal. As a minimum, the detector must be able to establish a temporal relationship between gamma-ray bursts and neutrino events with an accuracy of a few tens of seconds in order to establish this correlation. We will base our primary event selection on time coincidence using the directional information as a verification of the correlation with GRBs.

The time correlation is sufficient to determine a causal relationship between the neutrino signal and the gamma-ray burst. This is because we don't expect many "background" events satisfying our selection criteria for high-energy leptons - as shown in section 4.2 the chance background is  $\leq 3 \times 10^{-7}$ . The arrival-time of the gamma-rays may precede the arrival of the neutrino signal by a few seconds, or by many seconds. Or, the neutrinos may precede the gamma rays by a few seconds, depending on the details of the model and the intervening mass. The lower limit in coincidence duration over which we can search is set by the resolution on universal time stamping (both in NuBE and the satellites) or by the duration of the burst, whichever is longer. The upper limit (either forward or backward in time) is set by the background rate. The searchable coincidence interval must be at least 100 s, since a neutrino can be produced anywhere in the GRB duration. The upper limit will be determined by the arrival time difference distribution of uncorrelated events observed in the interval; we look at the distribution of GRB arrival time minus the neutrino signal arrival time for all of our

---

<sup>15</sup>37cm diam  $\Rightarrow \sim 10^4$  Ck photons along 37 cm length of track. At 300m from track, these 37 cm have spread to  $6 \cdot 10^6 cm^2$ , or  $0.0015 photons/cm^2$ . Each PMT has a projected photocathode area of  $1080 cm^2$  so on average it sees 1.5 photons. Each node thus sees  $16 \times 1.5 = 24$  photons. With an average QE of 20% and a conservative estimate of 50% overall collection efficiency (glass, silicon, interfaces) we expect  $\sim 3$  pe per node.

neutrino events and all of the GRB detected when NuBE is active.

Conclusions about the correlation may be more difficult if the time difference between gamma-rays and neutrinos is altered as a function of the distance from the GRB to the Earth. If this alteration is much larger than the universal-time resolution of the detector, we would have to plot arrival time difference divided by distance to the GRB to see a correlation indicative of different gravitational effects. This implies we would need a measurement of the distance to each GRB. Alternatively, since a few GRBs have been linked to known sources, a delay may yield a new astrophysical distance-measuring tool.

It may be that we measure some number of events and are unable to extract a time correlation function, able only to set limits on the coincidence rate. This would imply that neutrinos are not emitted in coincidence with the gamma rays at the energies predicted and to which NuBE is sensitive, or there is some fundamental misunderstanding of their propagation.

#### 4.1.2 Relative time for angular correlation

We assume that absolute-time correlation will identify GRB candidate neutrino events for us, and that we will verify their identity by pointing in the general direction of the identified GRB. The level of accuracy we must achieve will depend on our background rate. An angular correlation is approached in much the same manner as the time correlation, binning the events in their resolution bins and asking the probability of the events pointing, within resolution, to the GRB source. The relative time resolution within the detector must be a small fraction of the time it takes a photon or muon to traverse the array,  $\sim 1\mu s$ .

Events which leave signals in the NESTOR Tower provide good angular resolution because of the constrained geometry of the tower hardware and the higher detector density. The time resolution of  $\sim 5.5ns$  FWHM [Anassontzis02] suggests an angular resolution well below an rms of  $1 - 2$  deg for events with many signals in the tower.

#### 4.1.3 Track reconstruction for calibration on CR muons

Typical events in NuBE trigger at least 2 nodes by definition. Since these are separated by  $\geq 300m$  they provide a very long lever arm for pointing<sup>16</sup>. Since each PMT in a node has  $2.5ns$  time resolution, an event that fires

---

<sup>16</sup>time resolution of  $2.5ns$  leads to a potential for pointing accurate to  $\tan^{-1} = 0.0025/1 = 2.5mr$  for nodes on the same string, which share a common clock. The real

all 16 PMTs in a node can potentially have  $\leq 1ns$  resolution for that node. The two nodes on each string share a common clock, so their time jitter is dominated by the transit-time-spread of the PMTs, measured to be 5.5ns.

## 4.2 Event rates

Bahcall and Waxman [Waxman97][Waxman02] predict 10-100 observable muon neutrino interactions having energy  $\sim 10^{14}eV$  in coincidence with GRBs per year per  $km^2$  of detector area<sup>17</sup>. They point out that most GRBs will produce a single neutrino event in our detector, although nearby GRBs may produce 2 or more events in the duration of the GRB. We are not aware of any other quantitative estimate of the neutrino flux from GRB sources. We also may find events originating in atmospheric interactions and neutrinos from other galactic sources or AGNs. These may lead to as many as 10k multi-node events per year in NuBE, a result that would surely invigorate the construction of a larger and denser array such as KM3NET. Defining an event as a coincidence between 2 nodes, we find an energy minimum of  $\sim 65GeV$  for a muon traversing the 300m separation between nodes along a string. The measured muon flux at the NESTOR site suggests we will observe a downward-going muon rate of  $\sim 0.1Hz$  in each node, with many of these triggering both nodes in a string.

Random background rates can be calculated from measured coincidence rates in the NESTOR test floor [NESTOR-site]. As shown in Figure 15, the random rate for a 4-fold coincidence among 12 PMTs using a 1pe threshold is 0.25 Hz. This is the total 4-fold coincidence rate - it includes all background and all signals present at the site, so we know what to expect for our trigger rate. Correcting this for our 16 PMTs per node, the node-trigger rate will become  $\sim 1Hz$ . Our events require that at least two nodes trigger. This coincidence must occur within the transit time across the array,  $3\mu s$ : the rate of such coincidences in time is  $1 \times 1 \times 3 \times 10^{-6} = 3 \times 10^{-6}Hz$ . The probability of such a coincidence within any 100s time window is  $3 \times 10^{-4}$ . The GRB rate at Earth is  $\sim 300/yr) = 1 \times 10^{-5}/s$  or a probability of  $10^{-3}$  in any 100s interval. These are both random probabilities, so their combined probability is their product, or  $3 \times 10^{-4} \times 10^{-3} = 3 \times 10^{-7}$  as the chance of a random 2-node coincidence falling in the 100 second interval around a GRB time measured in a satellite.

---

resolution in this case will be limited by systematic effects such as from string position.

<sup>17</sup>Waxman has revised this to  $\sim 20$  events per  $km^2$ [Waxman02]

### 4.3 Background rejection

Background photons come from a constant  $K^{40}$  beta-decay and other radioactivity and from bioluminescence activity as shown in Table 3. The effects of  $K^{40}$  decay can be minimized by requiring coincidence between phototubes separated by distances much larger than the decay electron's range (see Figures 13 and 14). The effects of bioluminescence can be excluded based on the many coincidence level requirements, since it is typically "bursty" in nature, as shown in Figure 9. It is easy to distinguish bioluminescence from our signal. The total background photon flux has been measured at our site to give a 1/4 pe counting rate of  $\sim 50kHz$  for a 15 PMT [Aggouras1][NESTOR].

### 4.4 Calibration

Each PMT will be calibrated for single p.e. sensitivity. All node clocks will be calibrated to a relative accuracy that will allow us to reconstruct track directions based on photon arrival times at the nodes. The particle flight time from one node to another is  $1\mu s$  per  $300m$ ; the photon flight time is  $1.3\mu s$  for  $300m$ , since the index of refraction of water is  $n \sim 1.33$ . Relative timing accuracy between nodes of  $\leq 300ns$  is sufficient to provide rudimentary direction information. The two nodes on a single string will share a common clock and have relative timing accuracy better than 5 ns. LED events will be used to align all clocks and will occur at a rate of  $\sim 1/min$ .

All node clocks will be calibrated to an absolute accuracy of  $\leq 1s$  per year. This allows us to associate a neutrino observation event with a GRB whose arrival time and duration are known in absolute time to fractions of a second [SWIFT].

### 4.5 Monitoring

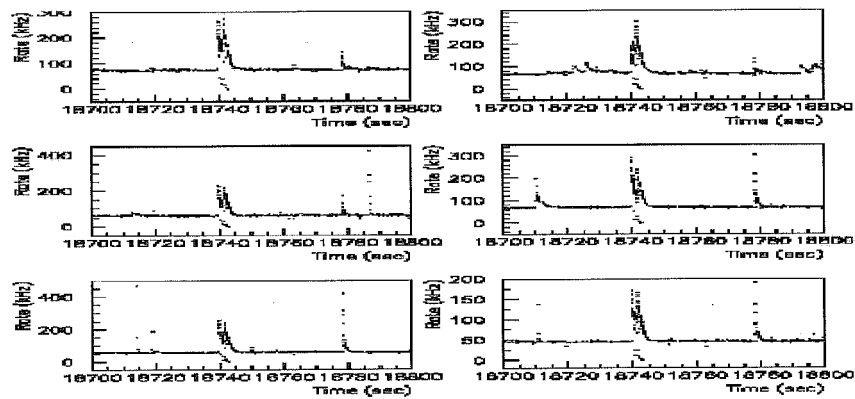
The NESTOR Tower and the NuBE strings are monitored continuously during deployment and in operation at the site. The Tower is connected to its junction box at the surface of the water and lowered into position, with monitoring during deployment provided through the shore cable. Data and housekeeping information flow continuously from the tower floors to the shore through separate fiber optic cables for each floor.

Near-real-time monitoring and quick-look data acquisition from each string is accomplished via acoustic links (see section 8.5). A duplex acoustic

## Bioluminescence Data from a depth of 4000 m

### PMT Rates vs Time

#### Up-Looking PMTs



#### Down-Looking PMTs

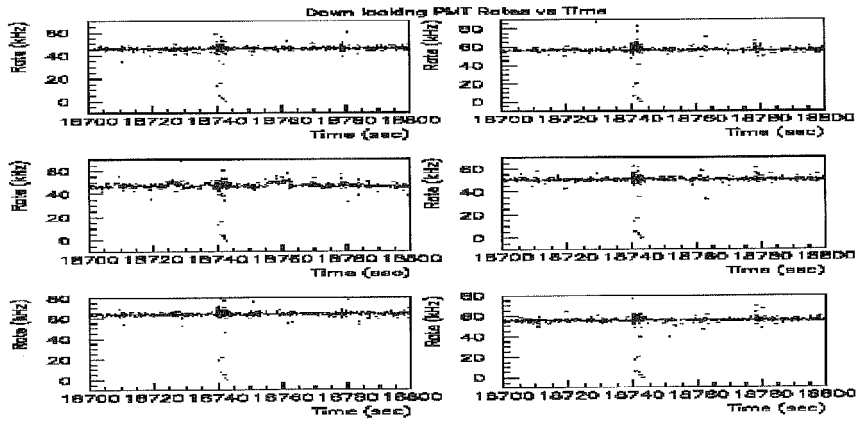


Figure 9: Bioluminescence measured at depth at the NESTOR site.

link connecting each node to the ship will serve for monitoring during deployment so that the operation can be aborted in case of a malfunction. A duplex acoustic link between each node and the Tower will be used for continuous monitoring and control at the site. The cluster’s Acoustic Module will also be used to measure relative position within the array, responding with a time stamp to each inquiry from transponders in the acoustic network. This position information will supplement the information obtained from timing the UV LED calibration pulses which are issued from each cluster once every 1000 seconds to synchronize clocks.

Each cluster’s Acoustic Module has access to the data from the cluster’s memory. Events having priority, such as those having a large number of hits, are recorded in a list so that these few events can be acoustically telemetered on command. This provides near-real-time access to selected events. In addition, housekeeping information including a digital monitor of the power level remaining in each power pack, tiltmeter, compass, and accelerometer is sent with the data to the Acoustic Module (see Table 6).

## 5 Optical Properties of Site

The optical properties of the site were measured in 1992 and 1994 using the best available technology at that time [Aggouras1][Anassontzis02]. These indicate a transmissivity ( $1/e$ ) of  $> 55m$  at a wavelength of  $460nm$ . However, since the Cherenkov light intensity increases at lower wavelengths (see equation 1), and the quantum efficiency of the PMTs peaks near  $400nm$  (see Figure 10), it is necessary to understand the transmissivity down to UV wavelengths where the water and the glass of the Benthos spheres cuts off transmission to the photocathode (see Figure 21).

### 5.1 Current Knowledge

Recent results in the literature indicate that the absorption length of light in clear ocean water is much larger in the near ultra-violet region than previously assumed [Pope]: as shown in Figure 11 the absorption length may be more than  $200m$  at wavelengths near  $400nm$ . If we convolute this curve with the Cherenov spectrum it suggests that an “effective” transmission length of  $\sim 110m$  is appropriate for our site for  $350 - 550nm$ . An excellent review of the existing literature of the absorption spectrum of pure ocean water in the visible and near-ultraviolet range can be found in Litjens et al [Litjens]. They point out that the data are in fairly good agreement above  $500nm$ , although variations of a factor of more than two exist throughout. Between

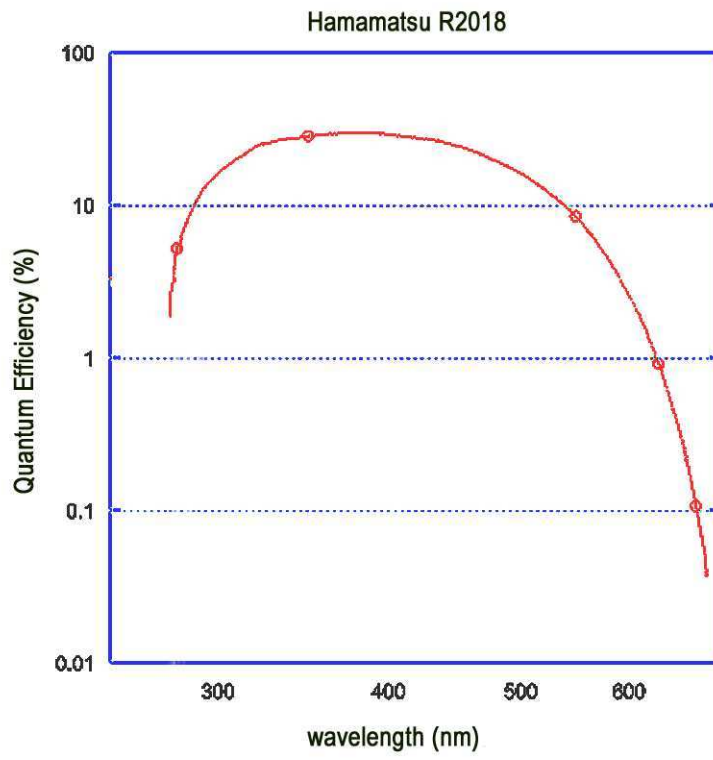


Figure 10: QE vs wavelength for the PMT we will use in NuBE.

about 300 nm and 500 nm, however, the data from different experiments varies by x50 or more. While the measurement for 460nm light was made *in situ*, and agrees with the literature values, for other wavelengths a sample was taken and measured in the laboratory using a monochrometer. Such measurements are suspect because of the effects of trapped gasses. Our *in situ* measurement will avoid this difficulty.

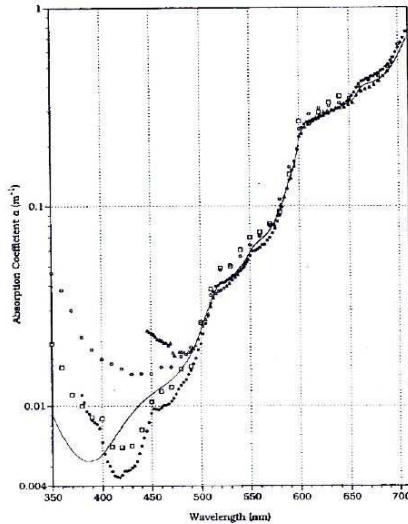


Figure 11: absorption coefficient vs wavelength for “pure” water, from Pope and Fry [Pope]. Note the wide divergence in “measurements” for wavelengths in the critical region of 350-550 nm.

## 5.2 In situ measurement using UV LEDs + PD

It is now possible to perform the measurement using simple LEDs and photodiodes (PD) at wavelengths, nearer the quantum efficiency peak of the PMT. LEDs are now available at 360 nm, 380 nm, 405 nm, 420nm, and 460 nm with bandwidths of  $\leq 5nm$ . A simple photodiode viewing the LED through a column of water at the site can be used to determine the local transmission coefficients. The system can be operated on batteries for many days, and so can be tested in air both before and after deployment. We propose to mount a set of 5 LEDs in a Benthos sphere with a battery operated driver that sequences through the 5 LEDs in a known repeating time structure. The current in the PD will be monitored 10 times each second

and digitized in a 12 bit ADC operating in the PMC slot of a laptop computer. The computer is fitted with additional battery packs to give it more than 72 hours of operating time. We propose to make measurements with 10m, 30m, and 100m separations, taking advantage of the easy deployment and recovery operations made possible by our NESTOR colleagues. This information will be used to optimize our detector design and LED monitor system.

## 6 Simulations and Detector Design

We have constructed a general simulation code and used this to design an array aimed at detecting  $10 - 100 TeV$  muons or electrons such as arise from neutrino interactions. Based on these simulations we have established a proposed detector design. We first describe the simulation code and then the design. Then we show effective area and sample signals.

### 6.1 Simulated Shower Signal

We have developed a Monte-Carlo code to simulate the detector response. To determine effective area the code grids the array mid-plane. A number of muon events,  $N_o$  (1000 or more), are passed through each point on the grid with incident directions randomly selected on a spherical surface. The light produced by each charged track is propagated to each PMT in the array to determine whether the PMT produces a p.e. This simulation includes the stochastic nature of the shower process, as indicated by GEANT (see Figure 8), the effects of absorption in the water, and the orientation and quantum efficiency of the photo-cathodes inside their Benthos spheres, and the transit time jitter of the PMT<sup>18</sup>. The arrival time of each photon that produces a photo-electron is recorded. The area added for each grid point is the number of triggers divided by  $N_o$  and multiplied by the area of the grid point.

Electron showers are simulated as isotropically emitting cylinders  $\sim 5m$  ( $\lambda_{rad} = 36cm$ ) in length with a total Ck photon count taken from a Gaussian distribution with mean and standard deviation taken from EGSnrc [EGS] simulations. Since it takes light  $\geq 45ns$  to cross a node, and since each node has expected TDC sensitivity of 2.5 ns per PMT, we will be able to measure the angle of the incident electron neutrino to an accuracy better than the  $14^\circ FWHM$  achieved in the NESTOR test floor [Aggouras2].

---

<sup>18</sup>measured to be 5.5ns for single pe's

	Rate(kHz)	photons <sub>-2s-1</sub>
$^{40}K$ decays in the sea water	24.0	114
$^{234}U, ^{235}U$ and $^{238}U$ decays in sea water	0.1	0
$^{40}K$ decays in the BENTHOS glass spheres	3.0	14
$^{40}K$ decays in the PMT glass	0.1	0
Thermionic noise	$7 \pm 1$	38
Luminous background	14.8	71
Total	50.0	237

Table 3: Calculated light intensities of several sources contributing to the baseline rate of an optical module having a 1/4 pe threshold.

## 6.2 Simulated Backgrounds

We also simulate noise in the detector. Sea and ocean water is known to contain  $K^{40}$  in concentrations that dominate the observed  $\sim 50kHz$  counting rate in a 15" diameter PMT feeding a discriminator having a threshold of 0.25 p.e. as measured at the NESTOR site.[NESTOR]

A  $^{40}K$  decay produces an electron of energy up to 1.3 MeV which can give a small burst of Cherenkov light as it ranges out in the water. The concentration of  $K$  in seawater is  $0.380g/l$ , the fractional abundance of  $^{40}K$  in the potassium is 0.0117

Other sources of photonic background include bioluminescence and other radioactive decays from trace elements, as shown in Table 3. These lead to an overall background rate of 50kHz at the single photoelectron level in our 15" PMTs at the site. More specifically the contribution from  $^{40}K$  has been calculated as 23.8 kHz and the contributions from  $^{238}U/^{235}U/^{234}U$  have also been calculated as 41.4 Hz, 2 Hz and 42.5 Hz respectively. The thermionic noise of the PMTs has been measured in the laboratory as approximately 8kHz. The remaining 18.1 kHz is attributed to D.C. bioluminescence [Bradner] [NESTOR]. In our simulations, the background is assumed to be poisson distributed with a mean rate of 10kHz appropriate for a 1 pe threshold.

## 6.3 Detector Design

Our proposed detector is an omnidirectional array of photo-sensitive nodes set in the 4km deep water at the NESTOR site. It is deep enough to shield from low energy cosmic ray backgrounds and to provide nearly isotropic

<b>Tower</b>	1	90m tall
floor (node)	4 per tower	30m separation in Tower
optical modules	12 per floor	
acoustic server	1 on Tower	
<b>Strings</b>	4	400m tall
nodes	2 per string	300m separation on string
clusters	2 per node	10m separation on string
electronics modules	1 per cluster	at center of cluster
optical modules	8 per cluster	5m spacing on square
acoustic modules	1 per cluster	
LED sphere	1 per cluster	

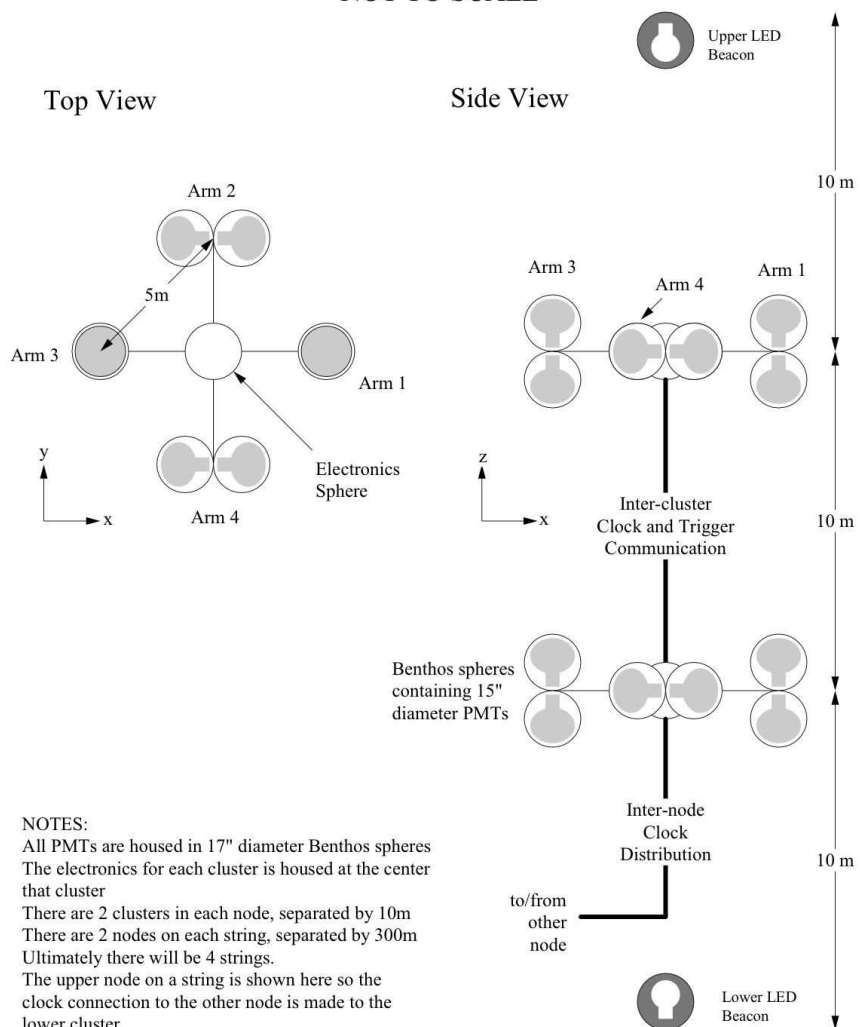
Table 4: NuBE / NESTOR Detector parameters

target mass for the high energy neutrinos. It takes a minimum of 2 TeV at the surface for a muon to reach 4km depth. The detector consists of 4 strings, 2 nodes per string, and the central tower of 4 floors, as shown in Figures 2 and 12 and described in Table 4.

Each string node consists of sixteen 15" diameter Hamamatsu photo-multiplier tubes (PMT). The PMTs are arrayed in two clusters per node, 8 PMTs per cluster. The PMTs are arranged in back-to-back pairs: 2 pairs have their photocathodes vertical, and 2 pairs have them horizontal. Each pair has full  $4\pi$  acceptance, with significant overlap because each photocathode is active over more than  $180^\circ$ . The spacing and orientation of PMTs is based on a Monte-Carlo study of  $^{40}K$  decays [NESTOR1] as illustrated in Figures 13 and 14 where the random coincidence from  $^{40}K$  and the coincidence due to the same  $^{40}K$  decay are displayed as a function of PMT separation for two different PMT orientations. Each cluster contains its own trigger, data acquisition, and storage system. Each cluster is thus a set of four  $4\pi$  PMT pairs with each pair having a photocathode area  $\geq 4400cm^2$ . The area projected onto any direction is  $\geq 1080cm^2$ . The two clusters in a node participate in a common trigger. The two nodes on a string share a common clock but otherwise the nodes are completely independent of each other.

Each tower floor has 12 PMTs, with pairs on the points of a hexagon, one PMT facing up and the other facing down. In our simulation the 6 downward facing PMTs form one cluster, while the 6 upward facing form another, giving 2 clusters per floor or node, just like the string nodes.

Schematic Diagram of a NuBE Node  
NOT TO SCALE



E.G. Judd 16th May 2006

Figure 12: Schematic diagram of NuBE node.

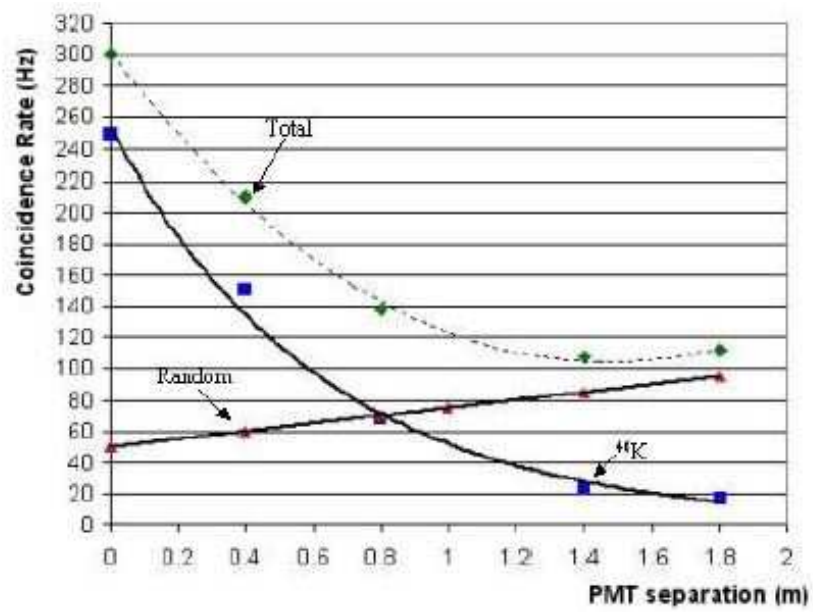


Figure 13: Coincidence rate between 2 PMTs having opposite orientations as a function of the separation distance between them. Random means coincidence from different  $^{40}\text{K}$  decays, while the other line shows the coincidence rate from the same  $^{40}\text{K}$  decay.

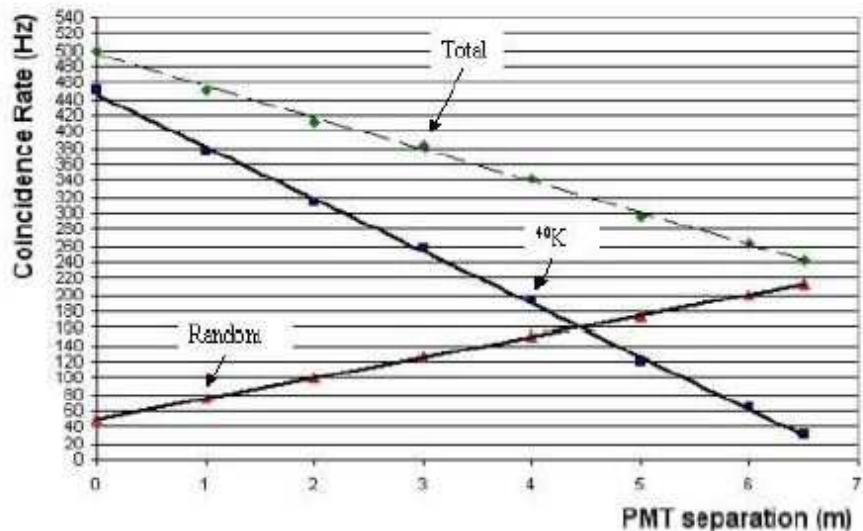


Figure 14: Coincidence rate between 2 PMTs having the same orientations as a function of the separation distance between them.(same as Figure 13)

If at least 1 p.e. is produced, the PMT is said to be hit. For purposes of simulation, at least two PMTs in each cluster of a node must be hit to produce a node trigger. Requiring a total of at least 4 hits per node reduces the random background below 1Hz [Aggouras2] and gives the effective area of  $\geq 1km^2$  at 100 TeV<sup>19</sup>.

## 6.4 Triggering

The PMT arrangement in a node leads to many events for which 6 or more PMTs fire of the 16 in the node: for some events, all 16 will fire. The hit distribution for NESTOR PMTs at the site is shown in Figure 15 from [Aggouras1]. Our trigger requires that a set multiplicity of PMTs within a node fire within 120 ns: this is set by the transit time across the node of ( $\sim 12m$  at 4.5 ns/m in either direction) and the clock interval (40ns). Figure 16 shows the arrival time distribution of shower photons at a cluster, with the first hit from a shower defining the 0 for that shower. Note that these distribution widths are dominated by the geometry of the detector -

<sup>19</sup>The 4-fold coincidence for 0.25 pe sensitivity has been measured for tower floors to be 3.76 Hz at the site. This is reduced by more than an order of magnitude if the threshold is raised to 1 p.e.

$\sim 60ns$  across, and demonstrate the idea that the Cherenkov light arrives in a very tight time window. This allows us to calculate effective area as a function of hit multiplicity within a time window.

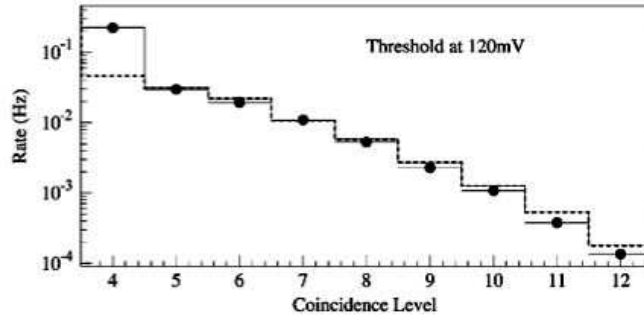


Figure 15: Coincidence rate for OMs as measured at the Site with 1pe thresholds [Aggouras1].

We define a minimum criterion for good events for GRB candidates to be the coincidence between any two nodes of our detector within the speed-of-light correlation time linking the two nodes ( $3\mu s$  max;  $1.3\mu s$  separating 2 nodes on a string). Any time the node triggers,  $5\mu s$  of hit timing information is recorded for each OM in the node. Our expected two-node signal including atmospheric backgrounds and all known source candidates<sup>20</sup> is  $< 10k$  events per year, or a random probability of  $< 0.03$  in the 100 s interval corresponding to the duration of a long GRB.

## 6.5 Acceptance

We use the simulation to generate events and set different trigger conditions to investigate our acceptance. Using the criteria we expect to employ for the trigger, at least two hits in one cluster with at least one hit in the other cluster in a node, and a total of four or more hits, we investigated the acceptance as a function of muon energy, node spacing and transmission length. The results are summarized in Figure 17. Note that we expect to find an effective transmission length of  $> 100m$  and expect to stage our nodes with 300m separation, indicating that our effective area will be  $\geq 1km^2$  for 10TeV muons.

We use the same methodology to calculate the effective area of a single node for single muons. This indicates an area of  $\sim 10^8 cm^2$  per node. Even

<sup>20</sup>none of which have yet been discovered at these energies

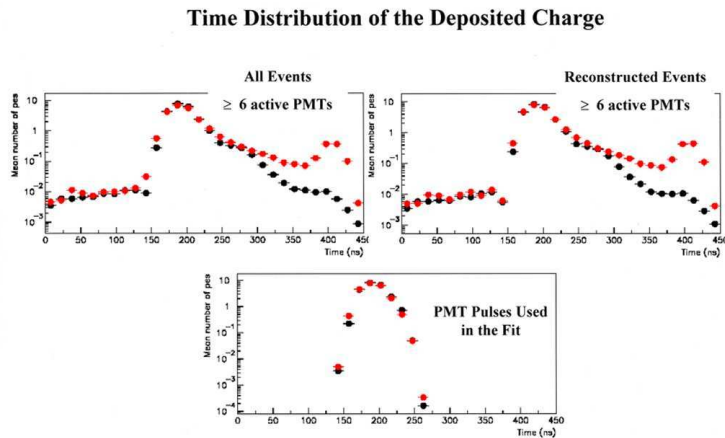


Figure 16: Arrival-time distribution as measured for photons hitting NESTOR PMTs at the Site [Aggouras2].

with an effective transmission length of  $50m$  our acceptance is  $\geq 0.5km^2$ , sufficient to detect 5 or more coincidences with GRBs in a measurement that has  $\sim 0$  background.

## 7 Data Analysis

The data analysis is all to be done off-line. Acoustic connections will provide quick-look data from the strings, samples of the data stream and housekeeping, but are not intended to provide large fractions of the data. The Tower will return a continuous stream that is bandwidth limited, using as loose a trigger as possible.

### 7.1 Data retrieval and archiving

There are two types of data in the data stream, event data and housekeeping data, as shown in Table 5 and Table 6.

The housekeeping data includes acoustic position data, total power status, local current. The event data includes all optical calibration data as well as the signals from low-energy muons and the real signal of interest,

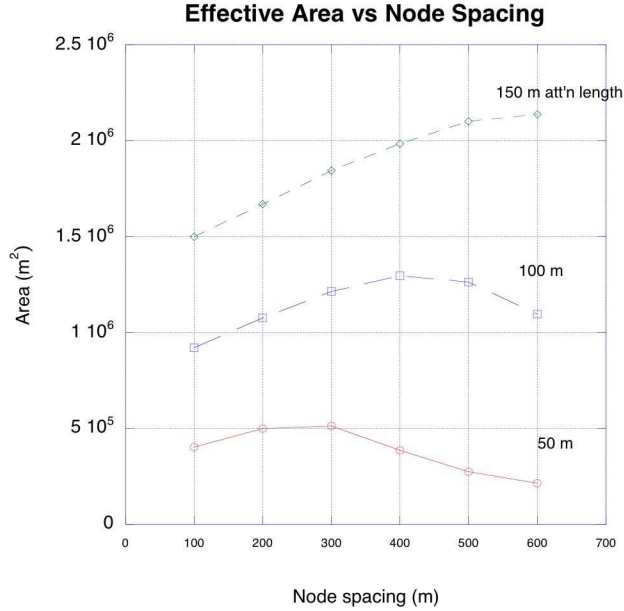


Figure 17: Acceptance as a function of node spacing for transmission lengths of 50,100,150m

that from high-energy particle showers. As described above, each node trigger causes  $\sim 70B$  of data to be written in each cluster of the triggered node. For calibration events, bursts of light from the local UV LED, only the node originating the calibration burst knows this is a calibration event. It sets a flag for the node trigger indicating a calibration burst. The other nodes do not know whether the trigger came from a real event or from a calibration pulse emitted by another node's calibration module. Off-line analysis must determine that.

## 7.2 Calibration

Absolute event time will be determined by comparing the value of the node clock counter with a universal time at the time of data retrieval. Since the counter was started at a known time, the overall time calibration can be easily established. Without periodic checks on the oscillators, the overall stability of  $\leq 10^{-7}$  would yield  $< 10s$  error over a one year period.

By periodically checking the local oscillator clocks with a reference clock, the requirement on the stability of the oscillators can be relaxed, although the VEC4 oscillators we have selected are stable to  $\leq 10^{-8}$  over periods

subsystem	bytes	total
header	10	
Time stamp	7	
Calibration flag	1	
Priority flag	1	
Counter TDCs	2 per TDC hit	variable

Table 5: Data event in NuBE cluster. If we record leading and trailing edges in each PMT (3 TDC/chn, 8chn/cluster) these give 96 bytes. Since we 0 suppress, and the noise rate is low, a typical event will have only a few hits and a length of 25-30B.

of many months. The Tower clock derives from a shore signal and is constantly corrected. Thus, periodic comparison between cluster clocks and the tower clock using the LED flashes can correct cluster times. We use 25 MHz oscillators because of their low power, high stability, and match to electronics clocking needs. The trigger condition (local coincidence within 120ns window) could change by 10% without significant change in trigger efficiency.

Calibration events will be easy to locate in the data because the node trigger rate is very small,  $< 1Hz$  at 1 p.e. threshold. We can locate a calibration event in the data stream of one node, and then search for triggers in other nodes occurring within  $20\mu s$  of the same UT. The light output of the LED calibration module is set to be sufficient so that all other nodes will trigger and record the flash. Using a small number of calibration pulses<sup>21</sup> the correct time difference can be determined and thus a running relative calibration of the node clocks can be performed. The time difference will be compared to the expected difference based on acoustic pulse timing to verify relative string positions.

### 7.3 Coincidence Analysis

Once the UT of each node trigger is established, all 20 data streams (16 string nodes plus 4 Tower floors) will be examined for coincidences within  $< 20\mu s$ , many times larger than the absolute maximum of the expected difference in response time (max  $3\mu s$ ). Each such multi-node coincidence will be examined for ideosyncracies, such as “unphysical” relative times.

<sup>21</sup>once per cluster per 1000s means once per minute for the 16 clusters + Tower )

subsystem	bytes
header	10
Time stamp	7
Priority flag	1
Scalers	72
Multiplicity scalars	48
Compass	4
Tilt angle	2x3
accelerometer	4x3
PS-HV level	4
PS - CC level	4
PS - AM level	4
Total	182

Table 6: Housekeeping event in NuBE cluster

Events passing all quality cuts will then be placed on a list of “good” events with their UT average value. We assume that the list will contain fewer than  $10^4$  candidates per operating year.

We expect a number of different kinds of events. The most common events are expected to be those where both triggered nodes are on a single string. If their relative times indicate downward going tracks, these will be primarily downward going cosmic ray muons. If their relative time indicates upward motion, they will be neutrino induced signals, of interest in themselves even without the GRB coincidence. We expect a number of events having 2 node triggers in different strings or in Tower nodes. These are also likely to be neutrinos because of the very long path length to the detector for horizontal trajectories.

The most exciting signals are likely to be multi-node triggers, those events that trigger more than 2 nodes. If they have a clear time-order, they are likely to be very high energy muon shower events. Their direction will indicate whether they are from extensive air shower remnants, or whether they were originally neutrino induced. If there is no clear directionality, they will be analyzed for consistency with an electron shower or muon-bundle origin. Since we expect our signal to come from very-high-energy shower events, this list will be the first searched for coincidence with the GRB events.

## 7.4 Comparison with Satellite Data

The UT list is then compared with a similar list generated by the satellite gamma-ray burst experiments. A distribution of time differences will result from subtracting the UT of the gamma-ray burst from the UT of the neutrino event. Peaks in this distribution constitute the potential signal. If we use 100s bins and the neutrino has 0 mass and the weak equivalence principle is obeyed we should see a peak in the first bin containing at least 10 GRB events, whereas the average population per bin should be  $\sim 0.03$ . Each of these events is then checked for relative node-to-node timing and for internal node timing to verify direction of origin. If this agrees with the satellite position, the identification is confirmed.

## 7.5 Non-GRB signals

Additional analysis of the node data will allow us to calibrate our detector by comparing the rate of upward-going and downward going events. Using only single muon tracks, as evidenced by their relative hit times unfolded as tracks, we can compare to the similar data from SuperK, a detector having vastly superior tracking possibilities.

# 8 Electronics

The basic electronics logic of the cluster is shown in Figure 18. The full set of electronics requirements are given in Appendix A.

We divide the electronics discussion into optical modules (OM), the electronics module (EM), the LED Calibration Module (LCM), the Power Supplies (PS), and the acoustic module (AM). The EM holds the Digitizing Trigger Board (DTB), data storage system (DSS), the Cluster Controller(CC), and the slow controls system (SCS). Each node acts independently of the other nodes. Each node consists of two clusters. Each cluster consists of 8 optical modules, 1 electronics module, 1 LED module, 1 acoustic module, and 2 power supplies as shown in Table 4. The wiring diagram is shown in Figure 19. Each OM sends its anode signal to the EM via copper cable. Each EM accepts 8 PMT anode inputs from its OMs. It also accepts an 8-line communications bus from the other EM in this node, a 2-line clock bus from the other node on this string, and an 9-line bus from its AM.

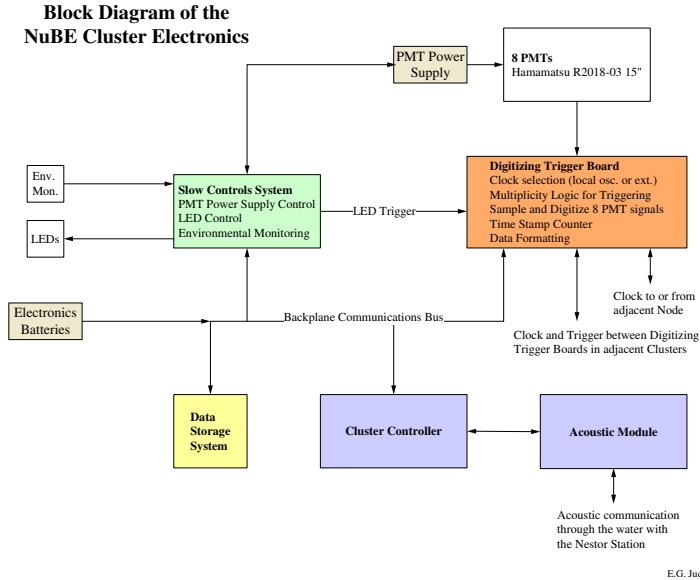


Figure 18: NuBE cluster electronics block diagram.

## 8.1 Optical Modules(OM)

Each Optical Module consists of a 17” diameter Benthos instrument-housing-sphere with a PMT and its base inside as shown in Figure 20 [Anassontzis02]. These borosilicate glass spheres are industry standard pressure vessels that transmit the wavelengths at which the photocathode has high efficiency (see Figures 21 and 10). Inside the sphere is a single 15” diameter photo-multiplier tube<sup>22</sup> with its 500MΩ base. Electrical power is brought into the sphere and the anode signal leaves the sphere through a 4-conductor connector. The spheres and PMTs are provided tested and ready by the NESTOR Institute<sup>23</sup>. This proposal includes funding for the connectors, base, and high-voltage (HV) supply. Each sphere is pressure tested to 500 atm. in water<sup>24</sup> at five stages, before, during, and after loading. The PMT is secured in place using silicon elastomer [Anassontzis02], and it has the back hemisphere covered by opaque material.

The high voltage for each cluster has a separate power supply (PS-HV)

<sup>22</sup>Hamamatsu R2018

<sup>23</sup>We need 128 OMs for our 16 clusters: 76 of these are ready for our new high-resistance bases. The other 52 have potted bases that need to be removed for our electronics.

<sup>24</sup>1atm = 14.5lbs/in<sup>2</sup> = 1053g/cm<sup>2</sup> so the pressure at 4km depth is  $4 \times 10^5 g = 380 atm$



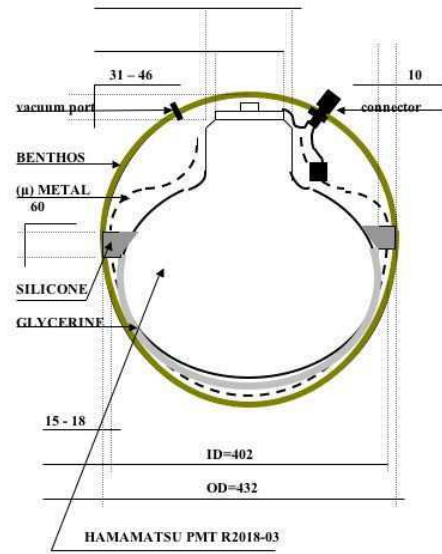


Figure 20: Schematic of an Optical Module showing mounting of PMT in a Benthos Instrument Housing sphere.

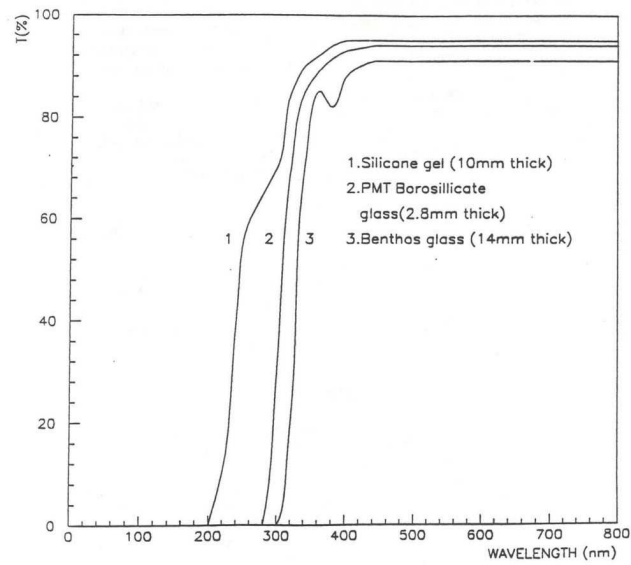


Figure 21: Wavelength dependence of light transmission in the housing, silicone, and PMT glass.

from the Electronics Module power supply (PS-EM). The PS-HV pack supplies  $\sim 250V$  chopped at 100kHz to a 12-stage Cockroft-Walton voltage multiplier in each OM that steps the voltage up to the 2300V DC required to operate the PMT. The HV source couples to the high-resistance base to provide very low power consumption ( $\leq 40mw$  per OM including the PS-HV power use) while still performing well for single photoelectron counting. We tested this design using an LED attenuated to produce single photons on the photocathode at 1 kHz in the presence of a second, randomly timed, multi-photon source operating at rates up to 200kHz, and found  $< 10\%$  variation in the single p.e. pulse height distribution.

## 8.2 Electronics Module (EM)

The electronics module houses the Digitizing Trigger Board (DTB), the data storage system (DSS), the Cluster Controller (CC), and the Slow Controls System (SCS). Power is brought in via a separate cable pair. Since the batteries deliver 3.6 V at 14C, all of our electronics are 3.3V standard inside the EM. The EM accepts anode signals from each of the 8 OMs in the cluster on twisted-pair electrical conductor which are routed to the Digitizing Trigger Board. A cable delivers a hit count from the Digitizing Trigger Board in one EM to the second EM in the node, and a separate cable brings the second EM hit count into the first EM. A cable connecting the two Digitizing Trigger Boards allows them to exchange triggers: each has a dedicated cable to send its trigger to the other DTB. A final cable allows the Digitizing Trigger Board to send its clock to the second DTB. In addition there is a cable that brings the clock to the first Digitizing Trigger Board from the other node on this string. A separate cable delivers data to the Acoustic Module. The wiring is shown in Figure 19.

### 8.2.1 Digitizing Trigger Board (DTB)

Each Optical Module sends the anode signal from its PMT to the Digitizing Trigger Board in the Electronics Module. The Digitizing Trigger Board consists of a three-threshold Time-to-Digital-Converter (TDC) system and a majority logic unit for the trigger as shown in Figure 22. The anode signal is fanned-out to three discriminators that have DAC-controlled thresholds: typically these will be set to 1.0 p.e., 2.0 p.e., and 5 p.e. The outputs from each discriminator go to a field-programmable-gate-array (FPGA) for processing. Within the FPGA, each discriminator signal is fanned-out to a 200ns delay line, a separate scaler channel for monitoring, and a pro-

programmable updating one-shot (an integral number of ticks of the system clock, nominally 120ns.). For triggering, the FPGA selects<sup>25</sup> one of the one-shots. This is called the hit signal for this channel. A section of the FPGA is programmed as a majority logic unit which determines hit coincidence level among its eight input “hit” signals: each multiplicity level has a separate scaler channel. A pair of lines goes from each Digitizing Trigger Board to its partner DTB in the other cluster of the node to deliver hit multiplicity (2 bits encode 0,1,2 or more).

The minimum trigger requirement is a “hit”, but this trigger type will be pre-scaled within the FPGA. Raising the hit constraint on the trigger<sup>26</sup> leads to decrease in both the signal and the noise. We expect to pre-scale the single hits and double hits but to keep every triple hit coincidence observed in which both clusters participate.

When a trigger is generated within a cluster it asserts an event trigger for the node. While the trigger decision is in progress the signal from each discriminator channel is working its way through a 200ns delay line and into a 400 MHz 16-bit counter. When a trigger is issued, the value of the counter is latched into a FIFO each time a leading or a trailing edge is encountered in a  $5\mu s$  window<sup>27</sup>. Note that the typical background rate is 10kHz per PMT for the 1 pe threshold, so the mean time between noise hits is  $100\mu s$ .

A typical single p.e. signal is approximately  $30ns$ . long: it will lead to latching 2 values from the counter, one when its leading edge arrives and one when its trailing edge arrives. A two p.e. anode signal would lead to a discriminator signal  $\sim 50ns$  in duration. The lowest counter value identifies the relative arrival time of the signal from that OM with respect to the time of the trigger decision. Note that this gives a record of all leading and trailing edges and therefore the time-over-threshold for all discriminators, an excellent measure of the total charge generated as pulses in the PMT. Latching the current value of the counter is accomplished at the leading edge of each clock tick, so the TDCs are always “live”: successive triggers would lead to a continuous record of the discriminator levels throttled only by available memory. The system with three discriminators all getting their leading and trailing edges recorded is a vey simple wave-form digitizer that operates on almost no power.

The trigger is issued by the FPGA at the leading edge of the next clock pulse if the event trigger line is asserted. Since a trigger leads to  $\sim 5\mu s$  of

---

<sup>25</sup>register selectable which one

<sup>26</sup>either raising the discriminator threshold or increasing the multiplicity requirement

<sup>27</sup>This window length is settable up to  $2^{16} * 2.5ns = 160\mu s$ , with  $5\mu s$  the likely setting.

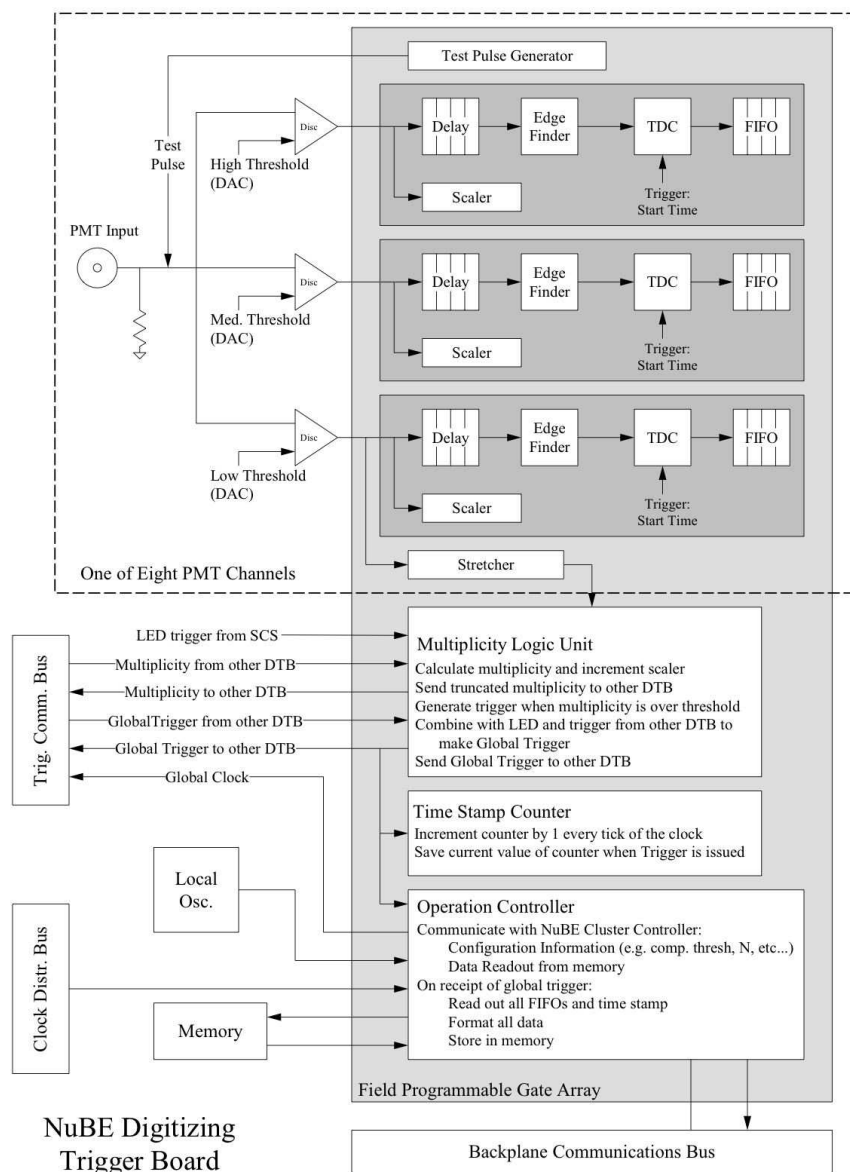


Figure 22: Block diagram of a Digitizing Trigger Board.

time record, triggers are disabled for a programmable number of clock ticks<sup>28</sup> following each trigger. Each trigger activates a list sequencer to read each of the counter FIFOs in the cluster and store its contents in data memory. If the original coincidence level met the priority condition<sup>29</sup> a priority flag is set and the event is added to a priority list for acoustic transmission. The priority events can be retrieved on command, sent to the local Acoustic Module and then to the server and to shore.

A straw-man definition of an event is shown in Table 5. Operating at 10Hz, we would record  $\sim 0.1GB/day$ . The data is stored directly in the Digitizing Trigger Board in fast onboard dual ported memory. Periodically the Cluster Controller will empty that memory into a flash memory for long-term storage. Each cluster's EM holds  $\geq 100GB$  of flash memory, sufficient for more than one year of continuous operation.

The relative arrival times of the anode signals within a node are recorded for each trigger to an accuracy of 2.5 ns in the 400 MHz counters. Since the transit time for a particle to cross the node along its axis is  $> 30ns$ , and for a photon is  $> 45ns$ , this crude TDC system provides enough information for most triggers to distinguish upward going from downward going tracks within a single node. This will allow us to compare flux recorded among the NuBE nodes and to compare upward going flux at each node to that in SuperK ([SuperK]) or in the NESTOR Tower.

There are two types of triggers, single-cluster triggers and two-cluster triggers. Both types lead to events, thereby causing each Digitizing Trigger Board to latch its hits and store them in the data memory. Single-cluster triggers are formed based on the number of hits present at the leading edge of the clock pulse in the FPGA. When a hit is present at the leading edge of the clock pulse a hit counter is incremented. Whenever this hit counter passes a selected pre-scale value, a trigger is issued. This is the equivalent of the minimum-bias trigger, and it most often leads to recording single hit events. There are 11 pre-scale values corresponding to hit multiplicities from 1 to 11. The pre-scale value for single hits will be set to allow  $\sim 0.001$  Hz of single-hit triggers.

Two-cluster triggers are the real physics triggers, and they require that at least two hits occur in one cluster in coincidence with any number of hits in the other cluster. Any time two or more hits are present in one cluster in coincidence with at least one hit on the lines from the other EM an event trigger is formed. This causes the event trigger line to go high. When the

---

<sup>28</sup>typically  $4\mu s$ . This option allows great test flexibility.

<sup>29</sup>typically multiplicity 4 or higher will get priority

cluster clock leading edge arrives, the FPGA issues a trigger signal initiating the latch-read-store sequence described above.

The FPGA will be programmed to keep a count of the number of times each discriminator fires, as well as a count of the occurrence of each multiplicity level in the cluster. These scaler values, 32 values of 4B each (128B total), will be read periodically as scaler events.

### **8.2.2 Cluster Controller (CC)**

The Cluster Controller is responsible for all data and command handling. It is the interface between the Acoustic Module and the Digitizing Trigger Board, the Data Storage System, and the Slow Control System. Commands can be delivered to the Cluster Controller from the acoustic module and data can be sent from the CC to the acoustic module via the copper connection. The Cluster Controller controls which of the flash memory units is active at any time.

### **8.2.3 Slow Controls System(SCS)**

We need to monitor voltage levels and detector orientation throughout the deployment, as well as temperature in the Electronics Module. To determine the detector orientation we will use a commercial compass having a standard readout. This will be used in conjunction with a tiltmeter and an accelerometer to detect changes in string positions. The slow controls units will communicate with the Cluster Controller via a commercial backplane. The Slow Control System will have a connection in the EM to allow firing the LED on command.

### **8.2.4 Data Storage System (DSS)**

All data will be stored in flash memory. A total of 100 GB will be used, in 8 GB segments, which will be activated as needed. This memory is on for a small duty factor, one segment only at any time, leading to very small power consumption.

## **8.3 LED Calibration Modules (LCM)**

Each cluster will have a separate LED sphere, the LCM, mounted 10m below the lower cluster or 10m above the upper cluster in each node. The LCM contains a set of the LEDs selected in our optical investigations at the site. The group of LEDs will irradiate  $4\pi$  to ensure detection at each node in the

Subsystem	Power	Notes
Optical modules	$\leq 0.32w$	CW Base $\leq 0.04x8$
Cluster Controllers	$\leq 0.1w$	
FPGA	$\leq 0.1$	trigger, data control, scalers
Discriminators	$\leq 0.06$	24 units (3 per PMT)
Oscillator	$\leq 0.01$	
Memory	$\leq 0.1$	100 GB flash
LED Modules	$\leq 0.01w$	(average; low duty cycle)
SCS	$\leq 0.01w$	low duty cycle
Total	$\sim 0.7w$	

Table 7: Power budget for single NuBE cluster

system. It will have a connection to the EM to allow firing on command with a settable amplitude.

#### 8.4 Power Supplies(PS)

The Tower has a direct power line from the shore which is capable of delivering many kW of energy at 300 V DC. This is converted to usable voltages through DC-DC converters. The Tower power operates four floors of PMTs with their controllers and data transmission, as well as the acoustic link coupling the strings to the shore.

Each string has 4 clusters, as well as an autonomous recovery system with two parallel acoustically triggered self-powered releases. Each cluster has three power supplies: one for the high-voltage (PS-HV), one for the electronics (PS-EM), and one for the acoustic system (PS-AM). These consist of packs of Li-ion batteries, selected for their high power density and long shelf-life.

As shown in Table 7, the average power consumption per cluster is  $\sim 0.7w$ , or 1.4 w per node. Each cluster will have  $\geq 7kwh$  of stored energy, providing a 15% contingency in power.

Operation of the acoustic data links and releases will take many watts for a few seconds periodically. These will each have a separate battery pack as supplied by the manufacturers guaranteed for multi-year lifetime at  $4^{\circ}C$ . The local temperature at the NESTOR site has been measured to be  $\sim 14^{\circ}C$ , so battery efficiency and response will be good.

## 8.5 Acoustic Modules(AM)

Each Acoustic Module is purchased from industry (e.g. DataSonics) and contains a battery pack and an acoustic modem in an independent pressure housing. An AM is mounted on the NESTOR Tower to act as the interface between the 16 cluster AMs in the acoustic net and the fiber optic cable to shore. The interface requires a special duplex RS232-to-optical converter to drive NuBE information from the acoustic network through the dedicated optical fiber to shore, and to receive commands from shore to convert to RS232 and thence to acoustic signals to the AM network.

On command, each cluster controller sends all events having a preset priority flag, along with a digital monitor of the cluster power available, to its acoustic module via RS232 protocols for transmission to the Tower acoustic module. Each AM is specified to have power to transmit 10B/s equivalent for one year. The data is actually transmitted on command to the server at a rate of 10 kB/s<sup>30</sup>.

We expect to read priority events such as those having 5 or more hits, and special “scaler” events, once every 16 minutes, cycling through the 16 clusters more-or-less continuously. We will set the priority flag for each local LED event so that we can more easily monitor oscillator and gain drift. We will also mark housekeeping events as priority for acoustic read-out.

## 8.6 Data acquisition(DAQ)

The primary data acquisition system is the Cluster Controller which periodically dumps the contents of the Digitizing Trigger Board memory onto the flash memory of the Data Storage System. A secondary path is used to store, on land, the data sent via the acoustic link to shore. Data coming in or going out on the fiber will be stored in time-order on a large disk farm on shore.

# 9 Mechanical Description of String, Node, and Cluster

The string, node, and cluster are shown in Figure 23. Each string consists of buoyancy, central rope (10 ton strength), four clusters in two nodes, dual parallel acoustic releases, and sacrificial anchor. Each NuBE node consists of two clusters of eight Optical Modules and associated electronics

---

<sup>30</sup>the unit has a maximum data rate of 17kB/s

and batteries separated vertically by 10 meters. The eight OMs of each cluster will be mounted on a frame and arranged to cover overlapping  $4\pi$  sectors of the field. Each of the clusters will be an independent entity with its own internal power supply, data controllers, data recorders, and acoustic modules. Floatation will be provided by groups of 17 inch diameter glass balls which provide 400 lbs of buoyancy each, with hardhats for mechanical protection; maximum string tension will be about 1,200 lbs. One hundred meters below the lower cluster there will be dual acoustic releases that will connect the string to a 2500 lb anchor. Upon an acoustic command from the ship, the release will disconnect the string from the anchor so that the instruments can float to the surface during the recovery.

The cluster must be able to attach to the string above and below: the string is continuous through the cluster and carries all of the weight. A load of 5000-10000 pounds may occur in the deployment during which the string will have to support the 2,500 lb anchor under dynamic conditions. Maximum steady loads when the string is installed will be about 1,200 lbs. The separation of the various components of the system provides a degree of protection in case of failure of any single element. The frame will be a structure comprised of 2 inch diameter aluminum alloy pipe. A total of 16 of these cluster frames will be needed for the deployment of the complete array. Frames such as these have been deployed at the site for over one year with no significant hardware degradation.

## 10 Deployment, Operation, and Recovery

There will be three separate deployment and recovery stages. In the first operation we will deploy a Site-Measurement-String. The 4-floor NESTOR Tower will already be in place at the site. The site-measurement string will include the LED-PhotoDiode transmission measurement system as well as a single Acoustic Module to test our acoustic communications. The Tower will be left in place after we have recovered the site string.

We will deploy a Prototype String (String 1) after analyzing data from the site-measurement string. We will construct this string based on what we have learned about the optics of the site. The cluster geometry is fixed, but the cluster-cluster spacing and the node-node spacing on this string will be optimized based on our measurements. String 1 will be left in place, working with the 4 floor Tower, for at least 3 months. We will then recover string 1, returning it to shore for analysis and recharging. We will then deploy the four NuBE strings, leaving them in place for at least 1 year of data taking,

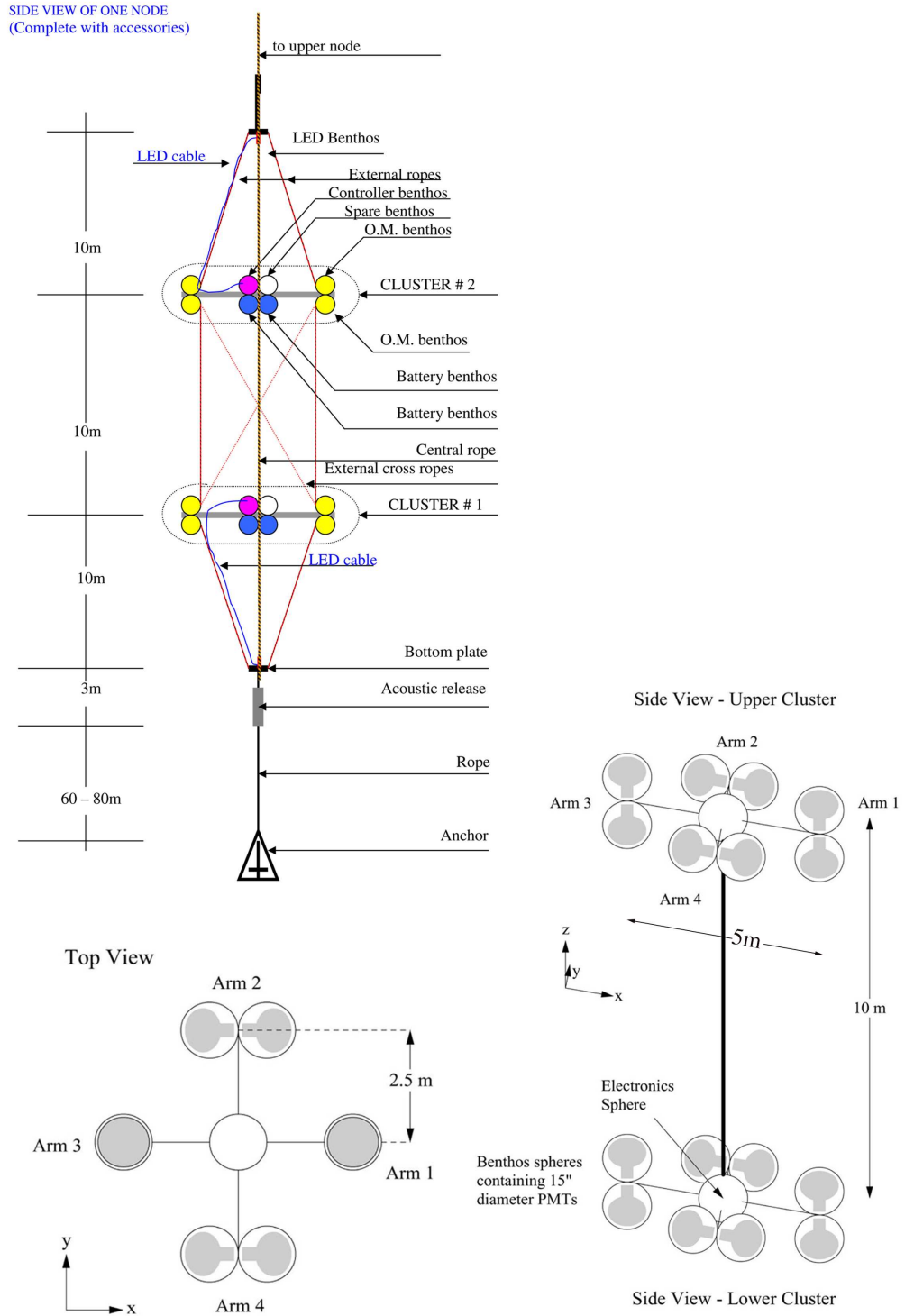


Figure 23: Mechanical diagram of a NuBE node. Two such nodes are mounted on a single string as shown in Figure 4.

in positions based on what we learned from the prototype string.

### 10.1 Site-Measurement String

The goals for this test are:

- refine the optical measurements between 350-450 nm. at the site.
- gain experience for novices operating at sea - ship, personnel, logistics.

In this test we plan to drop a string consisting of anchor, batteries, housekeeping (current, power levels), an acoustic module, and two Benthos Instrument spheres: one containing 5 LEDs with a sequencer and one containing a PhotoDiode with a laptop-resident data acquisition system. The Site-Measurement String will be up to 200m long, with the first optical instrument sphere 100 m above the anchor, and the second sphere ranging from 10m to 100m above that. Our NESTOR collaborators have already verified that there is no significant variation in optical properties once you are below about 2km in depth [Anassontzis94] [Khanaev], so we do not need to make our optical measurements over the full effective volume of the detector array. The Site-Measurement String will have sufficient battery pack to last 3 days at depth.

The LEDs in their sphere are pulsed in a known amplitude and duration pattern. Analysis of the patterns observed in the PD will yield the local optical properties at the five wavelengths chosen (360, 380, 405, 420, 460 nm). We will first deploy at 10m separation, then change to 30m, and finally 100m separation. We are able to do this because our NESTOR colleagues are experienced at string deployment and recovery. It is important to note that this will be a first deployment for many of our collaborators and will constitute an invaluable learning experience.

### 10.2 Prototype String

The goals for this deployment are:

- Place a Prototype String at the site.
- Verify the singles rates and coincidence levels in each cluster and in each node.
- Determine two-node coincidence rate.
- Determine coincidence rate with Tower.

- Verify robustness of our acoustic command and data link.

The purpose of this prototype string deployment is to verify that the NuBE OMs perform as expected from the NESTOR experience. We will verify the background in local coincidence mode, test our acoustic connections, and show that we can construct and operate a two-node string at the site.

The total power per node will be as in the final instrument. This will be provided by standard LiR battery packs.

We will communicate with this string in real time using the acoustic module to command the Cluster Controller to send priority data to the Tower and exercising the command link to alter priority definitions.

Once we have determined that the string is functioning properly we will leave it at the site for 3 months, monitoring it continuously through the acoustic link on the Tower. We will then retrieve the string and download all of its data for further analysis and comparison with the acoustically transmitted subset.

### 10.3 Four String + Tower array

The final array will consist of 4 strings plus the Tower as shown in Figure 4. These are to be deployed at the site in a square of  $\sim 600m$  diagonal<sup>31</sup>. Positioning of each string is not crucial, and an accuracy of 50-100 m is sufficient. After the tower is deployed, power and data will flow through the electro-optical cable to the shore. At a later time, the string deployment procedure may commence. First several transponders (minimum three) of the Long Baseline Acoustic Navigation System on the seabed of the site will be deployed. Then the transponder positions will be determined in absolute coordinates using a boat equipped with the required hardware and software (GPS, etc.). Once the String Anchor Point on the seabed (SAP) is decided, the string-deploying vessel (with Dynamic Position capability) will be positioned above it. The strings will be deployed using feedback from the transponders located on the string clusters, anchor and the seabed. Telemetry data from the string is continuously monitored through the acoustic connection for each cluster to the Tower acoustic module. The exact string deployment procedure will be decided after a detailed study of the size, weight in water and mass of the string components and anchor. Most probably we will deploy the string with the anchor (equipped with a transponder)

---

<sup>31</sup>this will depend on the optical measurements and performance of the single string with the tower

first followed by the rest of the string. The upper part of the string will be connected to a deployment rope with a release. The deploying vessel will take corrective action in order to minimize the effect of the underwater currents on the string and will place the string at the correct location. After the anchor touches the seabed, a release command will free the deploying rope from the string. The string is now deployed. After all four strings have been deployed they will be carefully and frequently resurveyed acoustically so that the relative distance of clusters and the tower will be known at any given time to an accuracy of better than 1 meter.

#### 10.4 Operations

Once the array is deployed, it is intended to operate with very little human interference. The frequent quick-looks at data and housekeeping events will allow us to send corrective commands quickly, such as to change a discriminator level to compensate for sagging gain. If a major failure occurs, such as the loss of a whole node, the collaboration would decide the best course of action. Most likely we would opt for recovery and repair, since its only a few miles from the shore and the Nestor Institute makes this straightforward. Since the Institute is actually constructing the strings, nodes, and clusters, the expertise for recovery and repair lies there also. We expect the strings to operate without direct interference for at least one year, although due to the proximity of the site to the shore and the availability of vessels it will be easy to recover, recharge, and redeploy every few months.

As part of our quality assurance we will have checklists for operation that require daily signatures noting such things as power levels, singles rates, and trigger rates. Most operations will be highly repetitive, and so accomplished under computer control, such as requesting priority data and housekeeping events from each cluster. NuBE's acoustic net is based on "pull" architecture: data is sent to the server only on request. Within each cluster, however, the data acquisition is a "push" architecture: events push into memory, not waiting for requests.

## 11 QA

Management for the Quality Assurance Plan is explicitly included in the planning and budget. The NuBE project anticipates a Preliminary Design Review and a Final Design Review conducted with non-project personnel. Documentation will include Requirements documents and Test Result documents clearly indicating how the requirements are being met. We expect

to stage the detector as noted above, learning at each stage for the next.

The QA Plan includes:

1. Each Optical Module will be measured for its sensitivity as a function of the impact parameter and angle of incidence on its surface for blue light.
2. Each OM will be tested at 500 atm in a tank prior to mounting on its cluster.
3. Each Calibration Module will be tested at 500 atm in a tank prior to mounting on its cluster.
4. Each Cluster will be tested on the bench prior to mounting in Node.
5. Each Node will be tested on the bench and then in shallow water in the Navarino Bay station prior to assembly on a String, activated by a Calibration Module.
6. Each String will be tested in shallow water in the Navarino Bay station prior to deployment, activated by a Calibration Module.
7. Deployment of Prototype String will test all concepts prior to Full Array String fabrication.
8. Each cluster and therefore each string will be continuously monitored during deployment with clear written criteria for aborting any activity and adjusting to anticipated situations.
9. A full recovery plan will be included in the deployment planning for each String.
10. Each String will have two parallel release mechanisms to better ensure string recovery.
11. Acoustic devices will be industry standard, tested to appropriate industry specifications.
12. All power routing will be industry standard for deep ocean applications.
13. All copper-based signal routing will be industry standard for deep ocean operations.
14. All housings will be industry standard for deep ocean operations, tested at 1.5x pressure at depth.

### **11.1 Single pe response**

The HV for each OM will be set in the laboratory to give a 1p.e. peak commensurate with the power and discriminator levels. Throughout the lifetime of the experiment, each OM will be monitored for drift in its 1 p.e. response.

### **11.2 DAQ tests**

Basic data acquisition functions will be tested in the laboratory including acoustic setting of priority conditions and other commands.

### **11.3 Acoustic tests**

The acoustic units will be tested in the laboratory and the 17 Acoustic Module network will be tested in the Navarino Bay at Pylos and in the nearby sea at 3000m depth prior to mounting on individual strings.

### **11.4 System tests**

Local ships are available to test all components in the Navarino Bay next (20 m, great beach) to the NESTOR institute.

## **12 Cost and Schedule**

We have a resource loaded project plan as shown the Gantt chart in Figure 24. We include all costs associated with the project, including simulation, design, fabrication, testing, operation, and analysis. We use a 20% contingency for the overall project, with some items having quotations as a basis of estimate having lower contingency, and some design items having 30% contingency.

### **12.1 Simulations**

We have included funding to cover the costs of further simulation work to refine our event reconstruction code and to continue array design efforts. This will include simulations using the full transmission function as well as better estimates of the shower development .

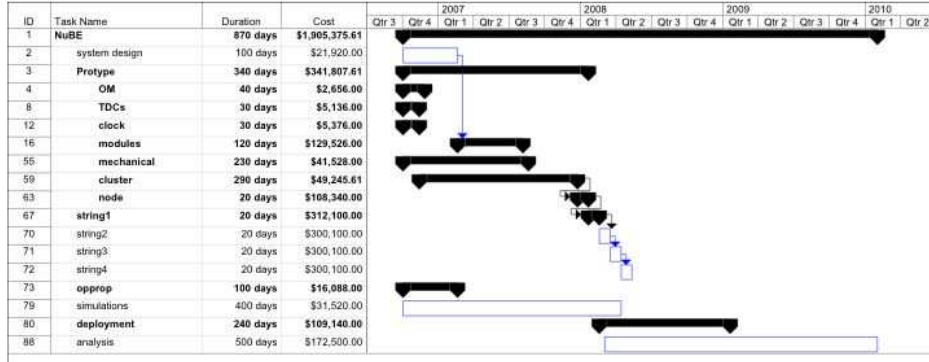


Figure 24: NuBE timeline based on fully resource loaded schedule.

## 12.2 String mechanical

The strings will be constructed in Pylos at the NESTOR Institute, where appropriate infrastructure and expertise reside. We have requested funding to cover costs of acoustic releases (2 per string for redundancy), for Benthos floatation spheres for buoyancy, for power supply and electronics housings, and for string and cluster mechanical parts. We also include funding for mechanical technician time to cover costs of string and cluster hardware fabrication and repairs.

## 12.3 Electronics

All of the detector electronics is funded by this proposal. Housekeeping devices (tilt-meter, compass, accelerometer) and battery packs can be purchased. We will also purchase the acoustic modules and server. We need to design and fabricate the PMT bases, high voltage systems, counter TDCs, scalers, control board, and acoustic-optical converter. We have requested funding to cover all aspects of this design, prototype, test and fabrication effort.

## 12.4 Deployments

We are fortunate to have access to all of the sea operations without cost to this program. We have requested funding for our participation in the deployments as experts tending our instruments. Also included are the expenses of laying out and surveying the acoustic grid which we will use in placing the final array. This includes purchase of the components of the

grid. Note that the operational costs of all deployment activities are borne by the NESTOR Institute.

## 12.5 Data analysis

The data analysis efforts begin prior to the first deployment, building on the code we developed for simulations of the detector response. The analysis will continue through the deployments, analyzing the quick-look data. The bulk of the analysis will take place after recovery of the strings, when we will analyze each node trigger. We expect to publish results within three years of the beginning of the project.

## 13 Glossary

- AM acoustic module - one per cluster
- CC cluster controller - one per cluster
- DTB digitizing trigger board - 8 channels, 3 counterTDCs per channel
- DSS Data Storage System- 100 GB flash memory per cluster
- EM Electronics Module - the housing for the DTB, CC, DSS, and SCS
- FPGA field-programmable-gate-array
- LiR Lithium Ion Batteries
- OM optical module - Benthos sphere housing R2018 15" PMT and base
- PS power supply - separate HV, EM and AM packs
- p.e. photo-electron
- SCS Slow Control System
- UT Universal Time

## References

- [Aggouras1] Aggouras, G. et al., NIM A552 (2005) 420.
- [Aggouras2] Aggouras, G. et al., Astropart.Phys. 23 (2005) 337.
- [AGN] Prothero, R.J., astro-ph/9612213; Mannheim, K. astro-ph/9703184
- [ANTARES] Aguilar, J. et al, astro-ph/0606229
- [AMANDA] Gross, A. and the Amanda Collaboration, astro-ph/0505278
- [Amati] Amati, L., et al., Astron. Astrophys. 390 (2002) 81
- [Anassontzis94] Anassontzis, E.G. et al., NIM A 349 (1994) 242
- [Anassontzis02] E.G.Anassontzis et al., NIM A479 (2002) 439.
- [anassontzis03] anassontzis, E.G., et al, Sea Tech. 44 (2003) 7;
- [AUGER] Mantsch, P et al, astro-ph/0604114
- [Band] Band, D. et al., Ap. J. 413 (1993) 281
- [BAIKAL] Wischniewski, R for the Baikal Collaboration, astro-ph/0507709
- [BATSE] Kaneko, Y. et al, astro-ph/0605427
- [Belli] Belli, B. Ap. J. 479 (1997) L31
- [Blandford] Blandford, R. & Znajek, R., 1977, Mon.not.Royal Astr. Soc. 179 (1977) 433
- [Bloom] Bloom, J., Frail, D., & Kulkarni, S., Ap. J. 594 (2003) 674
- [Bradner] H.Bradner et al., Deep-Sea Research v.34, (1987) 1831
- [Brand] Brandt, S., Lund, N., & Castro-Tirado, A., AIP Conf. Proc. 307 (1994) 13
- [Dar] Dar, A. 1998, astro-ph/9811196.
- [DUMAND] Wilkes, J. for the DUMAND Collaboration, astro-ph/9412019
- [EGS] EGSnrc home page <http://www.irs.inms.nrc.ca/EGSnrc/EGSnrc.html>
- [Lide] D.Lide (Ed.), Handbook of Chemistry and Physics, 81st edition, (2001) ch.11, p.57

- [Djorgovski98] Djorgovski, S., et al. *Ap. J.* 508 (1998) L17
- [Djorgovski99] Djorgovski, S., et al. GCN GRB Observation Report 189 (1999)
- [Fillipenko] Filippenko, A. *IAUC* (1998) 6969
- [Frail97] Frail, D., et al., *Nature* 389 (1997) 261
- [Frail01] Frail, D.A., et al., *Ap. J.* 562 (2001) L55
- [BEPPO] Frontera, F. astro-ph/0407633
- [Frontera] Frontera, F. et al. *Ap. J.* 540 (2000) 697
- [Galama98a] Galama, T. et al. *Nature* 395 (1998) 670
- [Ghandi96] Gandhi, R. et al., *Astropart. Phys.* 5 (1996) 81
- [Ghandi98] Gandhi, R. et al., *Phys. Rev. D* 58 (1998) 093009
- [HETE] Ricker, G.R. et al, *AIP Conf. Proc* 662, ed. G.R. Ricker and R.K. Vanderspek, NY AIP 3
- [ICECUBE] Ahrens, J. et al, *nestor-perfAstropart.Phys.* 20 (2004) 507
- [ICECUBE1] Ackermann, M. et al, astro-ph/0601397
- [Khanaev] S.A. Khanaev et al., *Proceeding of the 2nd NESTOR International Workshop*, p.253, L.K. Resvanis (ed.).
- [Kippen] Kippen, R. M., et al. *Ap. J.* 506 (1998) L27
- [Krauss] Krauss, L.M. and Tremaine, S. , *Phys. Rev. Lett.* 60 (1988) 176
- [KM3NET] Katz, U. astro-ph/0601012
- [Kulkarni98a] Kulkarni, S. et al., *Nature* 393 (1998) 35
- [Kulkarni98b] Kulkarni, S. et al., *Nature* 395 (1998) 663
- [Lamb] Lamb, D. et al., astro-ph/0505623
- [Learned] Learned, J.G. and Pakvasa, S. *Astroparticle Physics*, 3 (1995) 267
- [Learned and Mannheim] Learned, J and K. Mannheim, *Ann.Rev.Nuc.Part.Sci.* 50 (2000) 679

- [Litjens] Ronald A.J. Litjens, Terence I. Quickenden, and Colin G. Freeman, Applied Optics 38 (1999) 1216
- [Longo87] Longo, M.J. , Phys. Rev. D 36 (1987) 3276
- [Longo88] Longo, M.J. Phys. Rev. Lett. 60 (1988) 173
- [Macfadyen] MacFadyen, A., Woosley, S., & Heger, A., Ap. J. 550 (2001) 410
- [Matheson] Matheson, T. et al., Ap. J. 599 (2003) 394
- [Metzger] Metzger, M., et al., Nature 387 (1997) 878
- [Milgrom] Milgrom, M. and Usov, V.V. , Ap. J. 449 (1995) L39
- [NEMO] Distefano, D. et al astro-ph/0605067
- [NESTOR-site] Anassontsiz, E.G., et al, Sea Tech. 44 (2003) 7; Khanaev S.A. et al, Proceedings of the 2nd NESTOR International Workshop, page 253, L. K. Resvanis editor (1992);T.A.Demidova et al, ibid., page 284; E. Trimonis et al, ibid., page 321; I. F. Barinov et al, ibid., page 340
- [NESTOR] NESTOR Note 2006.30
- [NESTOR1] NESTOR Note 2006.001
- [Norris] J. Norris and J. Bonnell, Ap. J. 643 (2006) 266
- [Paczynski] Paczynski, B. and Xu, G. , Ap. J. 427 (1994) 708
- [Pakvasa] Pakvasa, S. Phys. Rev. D 39 (1989)1761
- [Pal] Pal,P. and D.P.Bhattacharyya, Can.J.Phys.63 (1985) 1050
- [Pandey] Pandey, S. et al, Astron. Astrophys. 417 (2004) 919
- [Perna] Perna, R., & Belczynski, K., Ap. J. 570 (2002) 252
- [Piro] Piro, L., in Gamma-Ray Bursts in the Afterglow Era, Springer, (2001) p. 97
- [Pizzichini] Pizzichini, G. Proc. 24th ICRC (Rome), OG2.1.8 (1995) p. 81
- [Plaga] Plaga, R. , Ap. J. Lett. 424 (1994) L9
- [Pope] Robin M.Pope andEdward S. Fry, Applied Optics 36 (1997) 8710

- [Roy] Roy, M. et al, astro-ph/9903231
- [Sakamoto] Sakamoto, T. et al., Ap. J. 602 (2004) 875
- [Soderberg] Soderberg, A. et al., Ap. J. 606 (2004) 994
- [Soffitta] Soffitta, P. et al., IAUC (1998) 6884
- [Stroh] Strohmayer, T. et al., Ap. J. 500 (1998) 873
- [SuperK] Abe, K for the Super-Kamiokande Collaboration, astro-ph/0606413
- [SWIFT] Gehrels, N. et al., ApJ. 611 (2004) 1005
- [Tavani] Tavani, M. , Ap. J. 497 (1998) L21
- [Vanderspek] Vanderspek, R. et al., astro-ph/0401311
- [Vanputten] van Putten, M. et al., Phys. Rev. D 69 (2004) 044007
- [Waxman95] Waxman, E. , Phys.Rev.Lett. 75 (1995) 386
- [Waxman97] Waxman, E. and Bahcall, J. , Phys. Rev. Lett. 78 (1997) 2292
- [Waxman02] Waxman, E. astro-ph/0211358
- [Weiler] Weiler, T. et al. 1994, hep-ph/9411432
- [Wijers] Wijers, R., Rees, M., and Meszaros, P., MNRAS 288 (1997) L51

## A Requirements

A complete set of requirements is available on our web site.  
<http://hena.lbl.gov/NuBE/index.html>

## B Cost Sharing

The NESTOR Institute will provide:

1. All tower hardware, sufficient to instrument four floors, excluding the central NuBE acoustic module.
2. 15 fiber optic connections to shore, 8 for tower floors, 1 for strings and 6 spare.
3. All power for tower and for NuBE acoustic pod on tower.
4. All ship time and all deployment related costs.
5. 140 fully tested optical modules consisting of 15" diameter Hamamatsu R2018-03 PMTs mounted in Benthos pressure housing with  $\mu$ -metal shields.
6. 20 housings for LEDs.
7. All necessary sacrificial anchors.
8. Local expertise and manpower for all mechanical design, fabrication, and testing of strings and clusters.
9. Office space for visiting science team members, including Gbit ethernet access to the internet.

This proposal will provide support for:

1. Design, prototype, fabricate, and test site measurement string, prototype string, and 4-string array.
2. All string hardware except the PMT's in their pressure housings. This includes rope, buoyancy, power supplies, cluster mechanical structures, electronics modules, acoustic modules, and positive release mechanisms.
3. All shipping and travel related expenses.
4. All data reduction expenses associated with the highest energy signals.